An Unsteady Total Variational Diminishing Axisymmetric Numerical Model for the Ram Accelerator Subsonic Combustion Thermal Choking Propulsion Mode

by

Peter Kaloupis

A dissertation submitted in partial fulfillment
of the requirements for the degree of

Master of Engineering

University of Washington

1990

Approved by _____
(Chairperson of Supervisory Committee)

Program Authorized
to Offer Degree _____

Date _____

In presenting this thesis in partial fulfillment of the requirements for the Master's degree at the University of Washington, I agree that the Library shall make its copies freely available for inspection. I further agree that extensive copying of this thesis is allowed only for scholarly purposes, consistent with "fair use" as prescribed in the U.S. Copyright Law. Any other reproduction for any purposes or by any means shall not be allowed without my written permission.

Signature _____

Date _____

University of Washington

Abstract

An Unsteady Total Variational Diminishing Axisymmetric Numerical Model for the Ram Accelerator Subsonic Combustion Thermal Choking Propulsion Mode

by Peter Kaloupis

Chairperson of the Supervisory Committee: Research Professor Adam P. Bruckner
Department of Aeronautics
and Astronautics

A Total Variational Diminishing (TVD) numerical model was developed to investigate the flow field about the ram accelerator projectile, and a simple heat addition model was used to model the subsonic combustion thermal choking propulsion mode. The ram accelerator is a ramjet-in-tube concept where a projectile resembling the centerbody of a ramjet flies through a tube filled with a premixed fuel/oxidizer mixture. The combustion process behind the projectile creates a pressure difference which provides a net forward thrust.

The present model solves the unsteady, two-dimensional, inviscid Euler equations, with a source term to account for the axisymmetric nature of the problem. The analysis is performed for an ideal gas, and a simple heat addition model is selected which attempts to model the physics of the combustion region. Comparison is made between the current numerical model and experiment.

Several problems are investigated, which include supersonic profiles of the ram accelerator with no heat addition, steady state heat addition, and unsteady heat addition, where the projectile is allowed to accelerate. Good agreement is found between the numerical model and the experiments for the case with no heat addition. The effects of the heat addition region on the unsteady calculations are also discussed. It was found that the method of heat addition selected was important in determining transient pressure profiles and accelerations for the ram

accelerator.

The numerical model developed gives the opportunity to investigate any projectile configuration and propellant mixture desired. In addition, it provides a method of investigating scaling effects and hybrid modes of propulsion, such as transdetonative modes of operation.

Table of Contents

List of Figures

ACKNOWLEDGEMENTS

I would like to express my sincere appreciation to my advisor Professor Adam P. Bruckner and to Professor Abraham Hertzberg for their guidance, encouragement, and financial support during the course of my studies at the University of Washington. They have influenced me personally as well as professionally. My appreciation also to Professor D. Scott Eberhardt who has helped me several times during the course of this thesis, and who permitted me the use of his equipment.

I would also like to thank my fellow graduate students who have labored with me on the ram accelerator. Their contribution to this thesis may not be directly measurable, but without them it would have been impossible. They are Carl Knowlen, Edward Burnham, Alan Kull, Gilbert Chew, Jackie Auzias de Turenne, Barbrina Dunmire, Amy Prochko, Andy Berschauer, and Robert Macintosh. In addition, I would like to thank the students of the University of Washington CFD Lab, in particular Linda Sigalla and Chen Chuck, who have helped me on many occasions with the machines and plotting routines. Thanks are also due to Alexey Pazhitnov and Vadim Gerasimov, who have helped me survive the slow spells.

Finally, I would like to thank my friend Dr. Moeljo Soetrisno for providing the original version on which the current code has been developed. His answers to my many questions were always helpful, and were for the most part patiently provided.

DEDICATION

Ramo Ergo Sum

It's not just a motto, it's a way of life.

Chapter 1

Introduction

The Ram Accelerator is a ramjet-in-tube concept developed at the University of Washington for accelerating projectiles to very high velocities [1-6]. It uses a propulsive cycle very similar to that of a conventional airbreathing ramjet. The projectile, which resembles the centerbody of a supersonic ramjet, travels through a tube filled with a premixed gaseous propellant, as shown in Figure 1.1. The tube acts as the outer cowling of the ramjet, and the combustion process travels with the projectile generating a pressure field which produces forward thrust. The gaseous propellant consists of premixed fuel and oxidizer, such as methane and oxygen, and selected diluents, such as carbon dioxide, nitrogen, or helium. The pressure, composition, chemical energy density, and speed of sound of the mixture can be tailored to maintain the desired level of acceleration and to optimize the ballistic efficiency. Here the ballistic efficiency is defined as the ratio of the rate of change of kinetic energy of the projectile to the rate of expenditure of chemical energy. There is no propellant or oxidizer onboard the projectile.

Such a device offers the potential for a number of applications, such as hypervelocity impact studies [7], direct launch to orbit of acceleration insensitive

payloads [8, 9], and hypersonic testing of vehicles and inlets.

Several modes of ram accelerator operation which span the velocity range of 0.7-12 km/sec have been proposed [1, 2]. These include the subsonic combustion thermally choked mode and several oblique detonation wave modes. The subsonic combustion mode is the most extensively studied experimentally, and has attained velocities of 2500 m/sec with a 70 g projectile in a 12.2 m long, 38 mm bore tube [4]. The oblique detonation wave mode has also been demonstrated experimentally [6], but will not be discussed here.

This work is intended to provide a numerical model for the analysis, and prediction of performance, of the ram accelerator in the subsonic combustion thermally choked mode of operation. The details of this mode will be presented in the following section. The details of the oblique detonation wave drive modes will not be discussed here, but they have been extensively treated elsewhere [6, 10]. To this end, the remainder of this thesis will discuss only the subsonic combustion mode, with reference to the other modes of propulsion where appropriate.

1.1 Background

In the following section the results of research on the ram accelerator are presented. Past experimental and theoretical work is highlighted, and justification is given for the assumptions of the current numerical model.

1.1.1 Experimental Work

The Ram Accelerator Facility

The ram accelerator facility which is described here was in operation until December 1989. Since that time the facility has been rebuilt and many subsystems have been updated. For a description of the new facility the reader is referred to Burnham, et al. [11]. The experiments that are described in this thesis were performed on the old system, and it is therefore the one that is described in detail here. The ram accelerator test facility is shown in Figure 1.2. It consists of a single-stage light gas gun, the ram accelerator test section, two dump tank systems, and a projectile catcher system. Associated subsystems are the gas handling system, the instrumentation, and the Data Acquisition System (DAS).

The 38 mm bore light gas gun is of conventional design, and is capable of accelerating a sabot/projectile combination (typical combined mass of 70-110 g) to speeds up to approximately 1300 m/sec. The muzzle of the gas gun is connected to a perforated-wall tube in the first dump tank system. This first tank system serves as a dump for the helium driver gas.

The ram accelerator test section consists of seven steel tubes with an inside diameter of 38 mm, an outside diameter of 100 mm, and a combined total length of 12.2 m. A total of 32 diametrically opposed instrument ports are distributed at 28 regularly spaced axial positions along the tube. Each of these instrumentation ports may hold piezoelectric pressure transducers, electromagnetic velocity transducers (copper wire coiled about a stainless steel core), or fiber optic cables. A 20- channel, 1 MHz DAS station is used to collect and store the data.

The ram accelerator tube is designed to operate at propellant fill pressures

of up to 50 atm. Thin mylar diaphragms are used to separate sections of the tube filled with different propellant mixtures. The fuel, oxidizer, and diluent gases are metered using sonic orifices and are routed to the appropriate section of the ram accelerator tube. This staging of propellant mixtures permits the operation of the ram accelerator to be optimized for a wide range of Mach numbers.

The ram accelerator test section is connected to a drift tube in the final dump tank system, where the projectile flies free. The tank has a pair of 25 cm viewing ports that allow for photographing the projectile while it is in free flight. A large diameter decelerator tube consisting of tightly packed carpet remnants is used to bring the projectile to a stop.

The Ram Accelerator Projectile

The nominal projectile configuration used in current experiments is shown in Figure 1.3. The projectile is fabricated from magnesium in two separate sections, the nose cone, and the body with integral fins. Both sections are hollow to reduce the overall mass of the projectile. A thin annular ring of magnetic material is place at the threaded joint between the nose and the body. This interacts with the magnetic transducers to provide absolute projectile position data, which can then be used to acquire a velocity history of the projectile and also to determine relative pressure wave position on the projectile with respect to the projectile throat. The overall length of the projectile is approximately 166 mm, and the throat diameter is 28.9 mm. The typical mass of the projectile ranges between 60-100 g, and the sabot mass is typically 13 g. The sabot is required in order to accelerate the projectile to the diffuser's minimum starting velocity.

Experimental Results

Experiments involving the thermally choked subsonic combustion mode of operation have been carried out using methane and oxygen as the fuel and oxidizer, and nitrogen, helium or carbon dioxide as the diluent. The diluent is used to tailor the speed of sound of the mixture so that the projectile is operating in the Mach number range of $M = 2.5 - 4.5$, and also to tune the heat release of the mixture so that a stable shock system can develop on the body of the projectile. When several such gas mixtures are used in succesive segments of the ram accelerator tube, reliable operation of the projectile results over a wide range of velocities.

Typical transducer outputs are shown in Figure 1.4. The top trace represents the magnetic transducer output. The first signal is due to the magnetic disc at the throat of the projectile passing the sensor, and the second is due to the magnetic disk at the base. This permits the determination of the exact position of the throat. The middle trace is from a pressure transducer located at the tube wall. It provides information about the location of the pressure waves with respect to the projectile.

This pressure trace is typical of the subsonic combustion mode. The first pressure pulse is generated by the oblique shock system in the diffuser section. A series of pulses then increase the pressure to its peak value, after which the pressure begins to decay. The increase in pressure after the initial oblique shock represents the normal shock system, which is assumed to be a complex system of oblique and normal shocks. The flow entering the combustion zone is subsonic. The decay in pressure following the peak pressure is due to the subsonic heat addition accelerating the flow to thermal choking, and the subsequent nonsteady

expansion of the combustion products behind the choking point.

The lower trace is the information recorded by the fiber optic cable. It shows the light emitted about the projectile and can be used to determine the location of the combustion region. The information provided by these sensors is used to generate a heat addition model for the current analysis.

1.1.2 Modeling and Numerical Work

Although several two dimensional numerical models exist for the oblique detonation wave drive modes [10, 12], none have been developed for the thermal choke mode of operation.

The models which currently exist for predicting the performace of the ram accelerator subsonic combustion thermal choking mode of operation are steady or quasi-steady in nature, and are restricted to one dimension. They do not include the effects of acceleration, as they solve the flow field as if it were in steady motion with respect to the projectile. The current model is essentially a "black-box" approximation, where the gasdynamic conservation equations are applied over the entire control volume, from the inlet to the thermal choke point behind the projectile. The amount of heat release is determined by the choking condition, which is determined a priori. This gives a good representation of the overall thrust and performance of the projectile, but provides no information about the flow field.

A nonsteady, pseudo-one dimensional numerical model has been developed by Burnham [13], who has investigated the transients associated with the starting process of the ram accelerator. He solves the pseudo-one dimensional Euler equations, but by the nature of the technique is not able to capture the oblique

shocks of the diffuser, or the details of the flow field.

In addition, all previous 1-D work does not model the discontinuous area change of the actual ram accelerator projectile, or the axisymmetric nature of the problem, which significantly alters the strength of the oblique bow shocks, and hence affects the final results.

1.2 Present Work

The purpose of this thesis is to develop a numerical code that can model the ram accelerator flow field properties and which, with simple heat addition, can model the subsonic combustion thermal choking mode. The present work is intended to resolve the flow field about the projectile, and to show the complex system of oblique shocks which actually determine the flow properties behind the throat, and the flow properties entering the subsonic combustion region. The code has the ability to model the heat addition crudely, and it is shown that the shock system can be generated on the projectile through the heat addition model employed. The amount of heat added is chosen to be in the range between the total heat available in the flow assuming complete combustion, and the Chapman-Jouget (C-J) minimum heat release necessary to support a shock.

Hence, even though the subsonic thermal choke mode can be represented, it is not strictly predictive of specific operating characteristics. The model does, however, provide a useful technique for observing trend characteristics and projectile configuration comparisons. With the addition of a combustion model the code can more accurately represent the physical problem.

The code, however, can accurately predict the flow field about the projec-

tile in the case of no heat addition. It also offers the potential for a much more physically correct model of the ram accelerator. With the inclusion of a non-ideal gas model and a combustion model, such as that being developed by Kull [14], it offers the potential for predicting the performance of the ram accelerator throughout its operating regime, including the effects of transition into different mixtures, and even different modes of operation, including transdetonative operation [11].

The two-dimensional Euler equations are solved, with the inclusion of a source term to account for the axisymmetric nature of the problem. Viscous effects, although important, are secondary effects at this point. Aside from the expense computationally, the inclusion of viscous terms requires an accurate representation of phenomena such as boundary layer transition and separation, as well as turbulence. These issues are too complex to be solved at this stage.

A multi-zone method is employed that can accurately capture the steep gradients of the flow properties associated with the discontinuous area change at the base of the projectile. The heat release is added as a source term to the flow behind the projectile, based on the heat addition model described in a later section.

The method employed to solve the Euler equations is second order accurate in space and time. It is a Total Variation Diminishing (TVD) scheme, and the time stepping is explicit in order to maintain time accuracy during the unsteady calculations. Such a scheme has the advantage of being able to crisply capture shocks and avoid spurious oscillations. This type of scheme is essential to capturing the steep gradients associated with the sudden expansion at the base region.

Chapter 2 gives a detail of the mathematical formulation of the problem,

and Chapter 3 discusses the numerical method employed to solve the equations. The initial conditions, boundary conditions, computational domain, and heat addition model are discussed in Chapter 4. The results of the current study are presented in Chapter 5, and Chapter 6 gives a summary of the results and conclusions, along with planned future work.

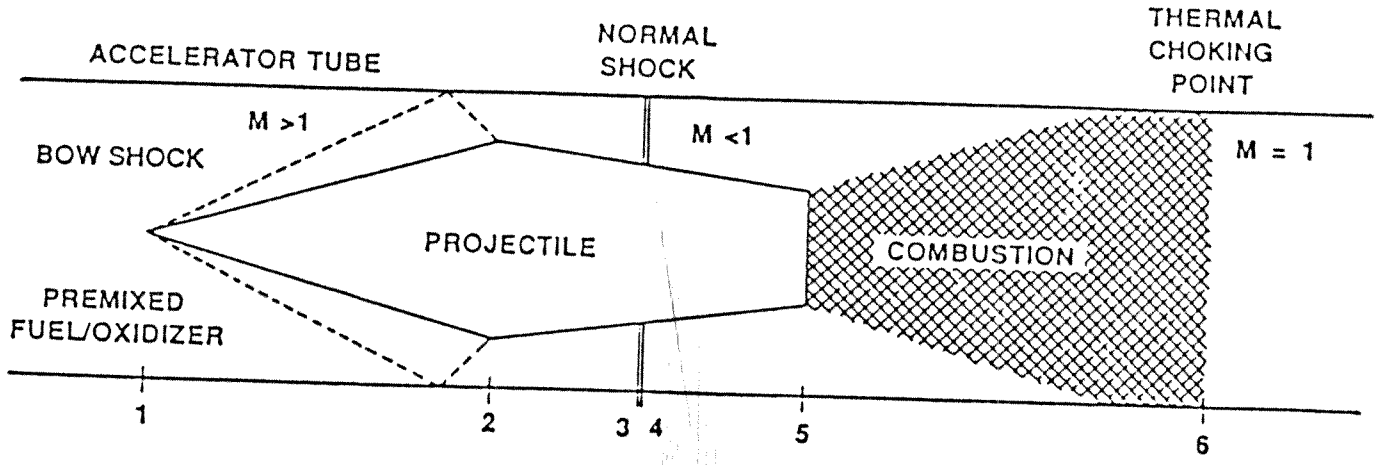

Figure 1.1: Subsonic Combustion Thermally Choked Ram Accelerator Mode

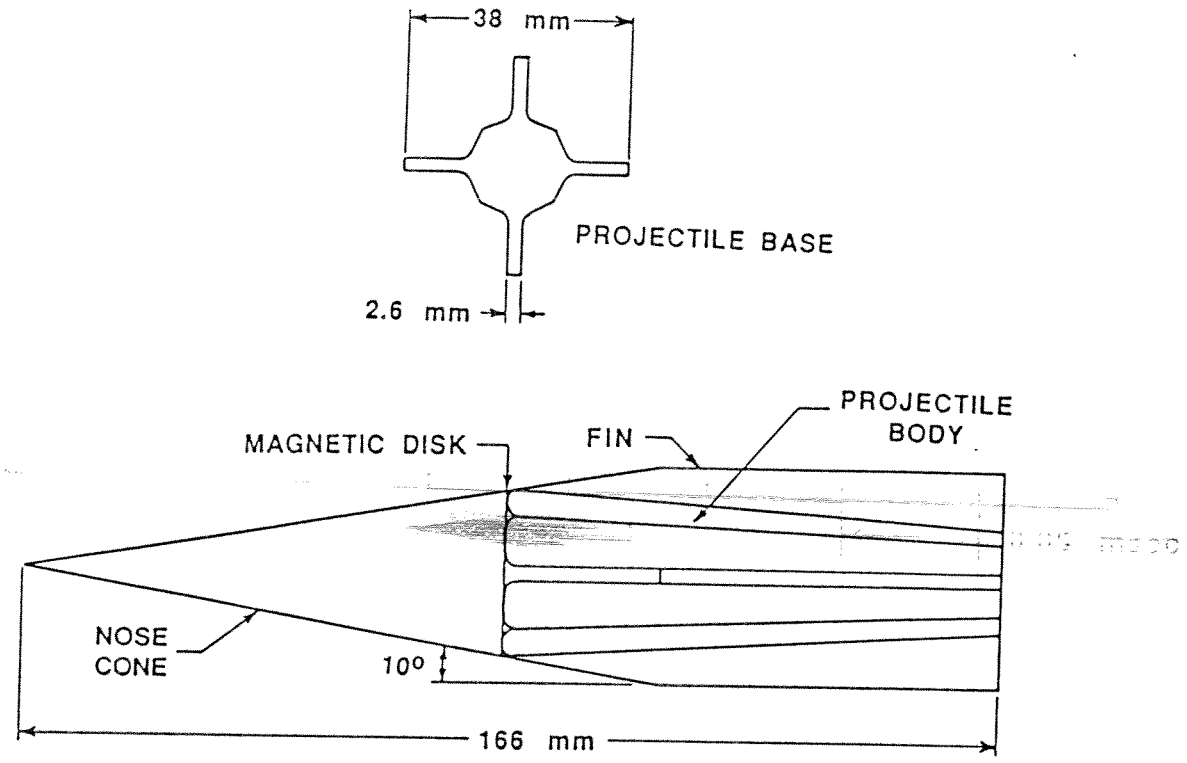

Figure 1.3: Ram Accelerator Vehicle Configuration

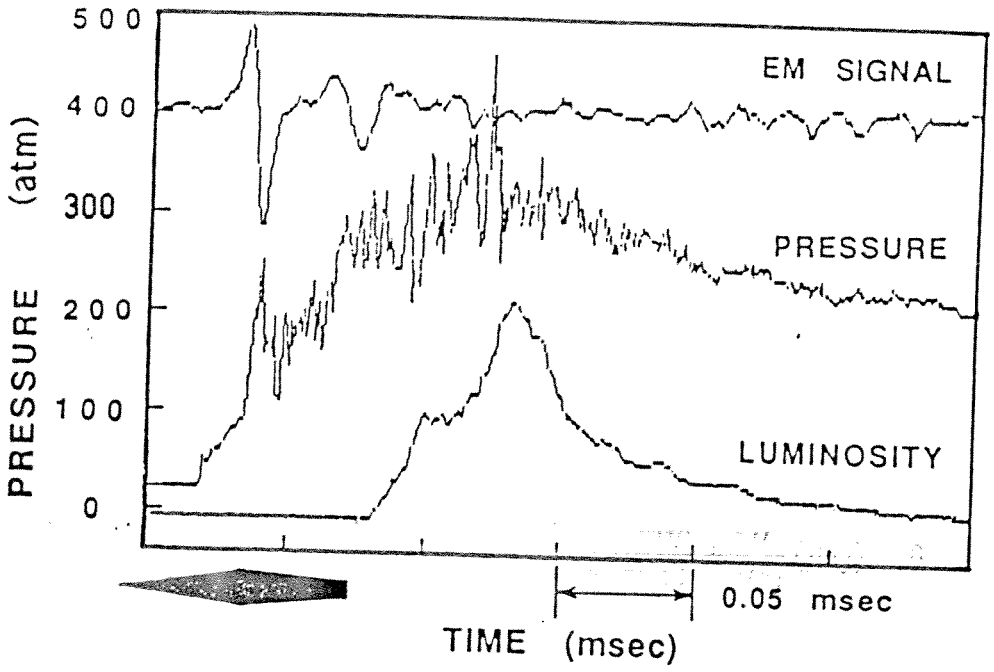

Figure 1.4: Typical Electromagnetic, Pressure, and Fiber Optic Transducer Signals in Thermally Choked Ram Accelerator Operation

Chapter 2

Mathematical Formulation

In this chapter, the governing equations of motion for the transport of fluid properties are presented. The Euler equations for the conservation of mass, momentum and energy are:

Conservation of mass

$$\frac{\partial \rho}{\partial t} + \frac{\partial}{\partial x_j}(\rho u_j) = 0$$

Conservation of momentum

$$\frac{\partial}{\partial t}(\rho u_i) + \frac{\partial}{\partial x_j}(\rho u_i u_j) = -\frac{\partial p}{\partial x_i}$$

Conservation of energy

$$\frac{\partial}{\partial t}\left(\rho\varepsilon + \frac{1}{2}\rho u_i u_i\right) + \frac{\partial}{\partial x_j}\left[\left(\rho\varepsilon + \frac{1}{2}\rho u_i u_i\right) u_j\right] = -\frac{\partial}{\partial x_i}(p u_i) \qquad (2.1)$$

where ρ is the density, u_i is the velocity component in i^{th}- direction, ε is the internal energy, and p is the pressure.

The Euler equations will be cast in conservation law form, so that shock waves and other discontinuities can be captured as part of the solution without special treatment. Lax [15] has shown that shock wave speed and strength are accurately predicted when the conservative form of the Euler equations is used.

2.1 Nondimensionalization of Variables

In order to avoid dimensionalized variables, the equations are normalized by the following parameters. The star $(*)$ quantities represent the nondimensionalized variables.

$$
\begin{aligned}
x^* &= \frac{x}{L} \\
y^* &= \frac{y}{L} \\
\rho^* &= \frac{\rho}{\rho_\infty} \\
u^* &= \frac{u}{c_\infty} \\
v^* &= \frac{v}{c_\infty} \\
p^* &= \frac{p}{\gamma p_\infty} \\
e^* &= \frac{e}{\rho_\infty {c_\infty}^2} \\
t^* &= \frac{t c_\infty}{L}
\end{aligned}
\tag{2.2}
$$

where e is the total energy per unit volume, c is the speed of sound, and the length scale L is the tube diameter. Hereafter the superscript $(*)$ is dropped, and all quantitites are assumed to be nondimensionalized.

2.2 Vector Form of The Euler Equations

The Euler equation set can be rewritten in vector form. To assure that discontinuities such as shock waves and contact surfaces can be captured as part of the solution without special treatment, the Euler equations are cast in strong conservation law form.

The two-dimensional Euler equations, written in cartesian coordinates, are as follows:

$$\frac{\partial Q}{\partial t} + \frac{\partial F}{\partial x} + \frac{\partial G}{\partial y} + H = W \tag{2.3}$$

where

$$Q = \begin{pmatrix} \rho \\ \rho u \\ \rho v \\ e \end{pmatrix}$$

$$F = \begin{pmatrix} \rho u \\ \rho u^2 + p \\ \rho uv \\ u\,(e+p) \end{pmatrix}; \qquad G = \begin{pmatrix} \rho v \\ \rho uv \\ \rho v^2 + p \\ v\,(e+p) \end{pmatrix}$$

$$H = \frac{1}{r}\begin{pmatrix} \rho v \\ \rho uv \\ \rho v^2 \\ v\,(e+p) \end{pmatrix}; \qquad W = \begin{pmatrix} 0 \\ 0 \\ 0 \\ \Delta H \end{pmatrix}$$

$$e = \rho\varepsilon + \frac{1}{2}\rho\left(u^2 + v^2\right) \tag{2.4}$$

Here, ε is the internal energy per unit mass, e is the total energy per unit volume, ΔH is the amount of heat added to the flow due to the combustion model, and the pressure, p, is determined from the equation of state

$$p = (\gamma - 1)\left(e - \frac{1}{2}\rho\left(u^2 + v^2\right)\right) \tag{2.5}$$

The equations describe the conservation of mass, momentum, and energy. The vector Q contains the conservation variables: mass, momentum, and energy, all per unit volume. The vectors F and G contain fluxes in the x and y directions, the vector H contains the axisymmetric term, with r as the radial dimension, and W contains the heat addition term.

2.3 Generalized Curvilinear Coordinates

The equations presented above are in cartesian coordinates. In general, it is desired that the equations be solved in a coordinate system more appropriate to the problem. The equations will be written in a generalized curvilinear coordinate system by transforming them from physical space to computational space. Figure 2.1 illustrates the one-to-one transformation from the physical space (x, y) to its corresponding computational space (ξ, η).

If a nonsteady grid can be defined by the transformations:

$$\xi = \xi(x, y, t)$$

$$\eta = \eta(x, y, t)$$

$$\tau = t \tag{2.6}$$

then to solve the Euler equations in the generalized curvilinear coordinate system without changing the equations themselves, Equation 2.3 must be transformable to:

$$\frac{\partial \tilde{Q}}{\partial t} + \frac{\partial \tilde{F}}{\partial \xi} + \frac{\partial \tilde{G}}{\partial \eta} + \tilde{H} = \tilde{W} \tag{2.7}$$

This can be done in the following manner, where to get the matrix transformations the chain rule must be used:

$$\frac{\partial Q}{\partial t} = \frac{\partial Q}{\partial \tau} + \frac{\partial \xi}{\partial t}\frac{\partial Q}{\partial \xi} + \frac{\partial \eta}{\partial t}\frac{\partial Q}{\partial \eta}$$

Expanding the other terms in a likewise manner gives the coordinate transformation matrix as:

$$\begin{bmatrix} \partial_t \\ \partial_x \\ \partial_y \end{bmatrix} = \begin{bmatrix} 1 & \xi_t & \eta_t \\ 0 & \xi_x & \eta_x \\ 0 & \xi_y & \eta_y \end{bmatrix} \begin{bmatrix} \partial_\tau \\ \partial_\xi \\ \partial_\eta \end{bmatrix} \tag{2.8}$$

The inverse transformation can be derived in a like manner, where

$$\begin{bmatrix} \partial_\tau \\ \partial_\xi \\ \partial_\eta \end{bmatrix} = \begin{bmatrix} 1 & x_\tau & y_\tau \\ 0 & x_\xi & y_\xi \\ 0 & x_\eta & y_\eta \end{bmatrix} \begin{bmatrix} \partial_t \\ \partial_x \\ \partial_y \end{bmatrix} \tag{2.9}$$

Since these transformations are inverses of each other we can obtain

$$\begin{aligned} J^{-1} &= x_\xi y_\eta - x_\eta y_\xi \\ \xi_t &= J\left(-x_\tau y_\eta + y_\tau x_\eta\right) \\ \eta_t &= J\left(x_\tau y_\xi + y_\tau x_\xi\right) \\ \xi_x &= J y_\eta \\ \xi_y &= -J x_\eta \\ \eta_x &= -J y_\xi \\ \eta_y &= J x_\xi \end{aligned} \tag{2.10}$$

Here x_ξ, x_η, y_ξ, y_η are calculated using second order differencing by assuming $\Delta\xi = \Delta\eta = 1$. The terms ξ_x, η_x, ξ_y, η_y are the grid metrics.

Now that the grid transformations are known, the final conservation form of the Euler equations in generalized curvilinear coordinates can be given. Expanding the Euler equations using the chain rule we get:

$$\frac{\partial Q}{\partial \tau} + \xi_t \frac{\partial Q}{\partial \xi} + \eta_t \frac{\partial Q}{\partial \eta} + \xi_x \frac{\partial F}{\partial \xi} + \eta_x \frac{\partial F}{\partial \eta} + \xi_y \frac{\partial G}{\partial \xi} + \eta_y \frac{\partial G}{\partial \eta} + H = W \tag{2.11}$$

This equation is not in divergence form, therefore it is not conservative. It can be put in conservative form by multiplying through by J^{-1} and then differentiating by parts as follows:

$$J^{-1}\xi_x \frac{\partial F}{\partial \xi} = \frac{\partial}{\partial \xi}\left(J^{-1}\xi_x F\right) - F\frac{\partial}{\partial \xi}\left(J^{-1}\xi_x\right)$$

Applying this to all the terms and making use of the grid metrics the equation can be written in divergence form as:

$$\frac{\partial \tilde{Q}}{\partial t} + \frac{\partial \tilde{F}}{\partial \xi} + \frac{\partial \tilde{G}}{\partial \eta} + \tilde{H} = \tilde{W}$$

where $\tilde{Q} = J^{-1}Q$, $\tilde{F} = J^{-1}\left(\xi_t Q + \xi_x F + \xi_y G\right)$, $\tilde{G} = J^{-1}\left(\eta_t Q + \eta_x F + \eta_y G\right)$, $\tilde{H} = J^{-1}H$, $\tilde{W} = J^{-1}W$. If the superscript ($\tilde{}$) is dropped from the expression, the equation can be rewritten as:

$$\frac{\partial Q}{\partial t} + \frac{\partial F}{\partial \xi} + \frac{\partial G}{\partial \eta} + H = W \tag{2.12}$$

which is of the form required, with

$$Q = J^{-1}\begin{pmatrix} \rho \\ \rho u \\ \rho v \\ e \end{pmatrix}$$

$$F = J^{-1}\begin{pmatrix} \rho U \\ \rho u U + \xi_x p \\ \rho v U + \xi_y p \\ U\left(e+p\right) \end{pmatrix}; \qquad G = J^{-1}\begin{pmatrix} \rho V \\ \rho u V + \eta_x p \\ \rho v V + \eta_y p \\ V\left(e+p\right) \end{pmatrix}$$

$$H = \frac{J^{-1}}{r}\begin{pmatrix} \rho v \\ \rho u v \\ \rho v^2 \\ v\left(e+p\right) \end{pmatrix}; \qquad W = J^{-1}\begin{pmatrix} 0 \\ 0 \\ 0 \\ \Delta H \end{pmatrix}$$

and

$$J^{-1} = x_\xi y_\eta - x_\eta y_\xi$$

$$U = \xi_t + \xi_x u + \xi_y v$$

$$V = \eta_t + \eta_x u + \eta_y v \tag{2.13}$$

Here J is the Jacobian matrix, and U and V are the contravariant velocities which are parallel to the grid lines, but are not necessarily perpendicular to each other.

The unsteady Euler equations are hyperbolic for all Mach numbers, and solutions can be obtained by using a marching process in time. The two-dimensional Euler equations have three different characteristic speeds, u, $u + c$, and $u - c$. In supersonic flow all three characteristics are positive, so information can only travel downstream. In subsonic flow however, the $u - c$ characteristic becomes negative and information can propogate upstream.

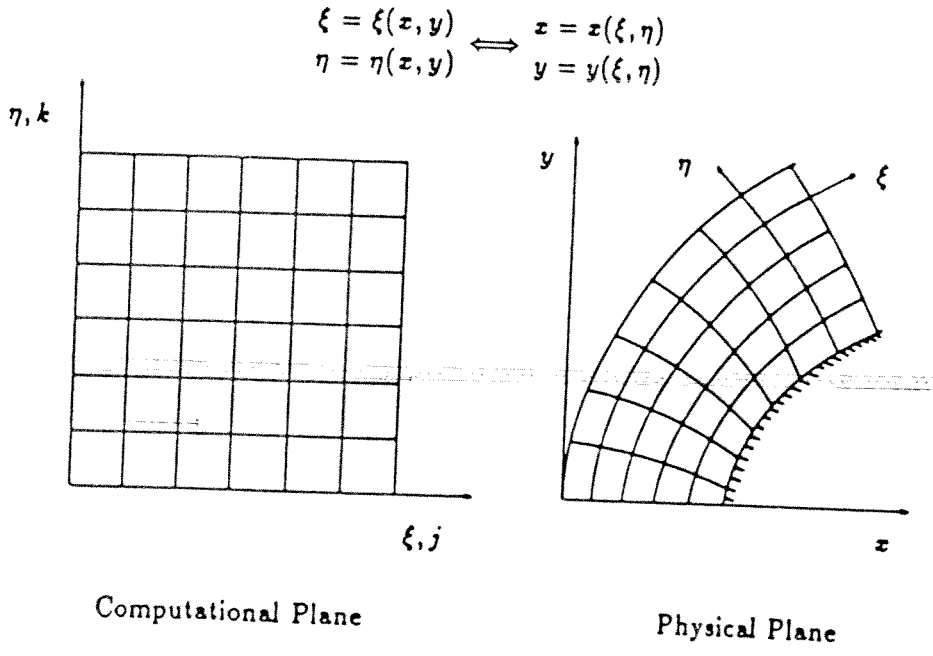

Figure 2.1: Transformation from Physical Space to Computational Space

Chapter 3

Numerical Method

The Euler equations are cast in conservation law form so that any shock waves and contact surfaces are captured as part of the solutions without special treatment. This technique is called shock capturing. Lax [15] showed that the physically correct weak solutions corresponding to the Rankine-Hugoniot equations are correctly predicted when the conservative form of the Euler equations is used.

Roe [17] and Yee, Warming, and Harten [16] considered a new class of schemes which are more appropriate for the computation of weak solutions (ie, solutions with discontinuities). These schemes are required to be total variational diminishing in the nonlinear scalar and constant coefficient system cases, and are consistent with the entropy inequality and with the conservation laws. Since they are total variational diminishing, they are guaranteed not to generate spurious oscillations. Consistency with the entropy inequality and conservation laws ensure the weak solutions are physical solutions. This class of schemes is called Total Variational Diminishing (TVD).

3.1 Total Variational Diminishing Scheme

Total Variational Diminishing (TVD) is a mathematical definition which describes a specific property of a scheme. TVD schemes were originally derived for nonlinear scalar equations and constant coefficient systems of equations, and have been extended for nonlinear systems of equations, i.e., hyperbolic conservation law systems. To date, there is no formal extension of the TVD schemes to nonlinear systems of equations and hence no guarantee of monotonicity of the solutions. However, the TVD schemes generally do an excellent job of smoothing out numerical oscillations near shocks. The TVD scheme used in the present work is the second order scheme of Yee, Warming and Harten [16].

The definition of total variational diminishing is given by:

$$TV(Q) = \sum_{j=-\infty}^{j=\infty} |Q_{j+1} - Q_j|. \tag{3.1}$$

If a scheme is TVD then

$$TV\left(Q^{n+1}\right) \leq TV\left(Q^{n}\right) \tag{3.2}$$

where Q is the conservative variable. A procedure which produces an explicit TVD scheme is summarized briefly below.

First, the flow vectors are manipulated and split into positive and negative running characteristics. To split the flux vectors, the equation may be put into a non-conservative form:

$$0 = \frac{\partial Q}{\partial t} + \frac{\partial F}{\partial \xi} + \frac{\partial G}{\partial \eta}$$

$$0 = \frac{\partial Q}{\partial t} + \frac{\partial F}{\partial Q}\frac{\partial Q}{\partial \xi} + \frac{\partial G}{\partial Q}\frac{\partial Q}{\partial \eta}$$

$$0 = \frac{\partial Q}{\partial t} + A\frac{\partial Q}{\partial \xi} + B\frac{\partial Q}{\partial \eta} \tag{3.3}$$

where F and G are the flux vectors and A and B are the flux Jacobian matrices. Second, to split the flux vectors into positive and negative running characteristics, the Jacobians are diagonalized as follows:

$$0 = \frac{\partial Q}{\partial t} + \left(X\Lambda X^{-1}\right)_A \frac{\partial Q}{\partial \xi} + \left(X\Lambda X^{-1}\right)_B \frac{\partial Q}{\partial \eta}$$

$$0 = \frac{\partial Q}{\partial t} + \left[X\left(\Lambda^+ + \Lambda^-\right)X^{-1}\right]_A \frac{\partial Q}{\partial \xi} + \left[X\left(\Lambda^+ + \Lambda^-\right)X^{-1}\right]_B \frac{\partial Q}{\partial \eta} \tag{3.4}$$

where Λ_A and Λ_B and X_A and X_B are the eigenvalue and the right eigenvector matrices of the flux Jacobians in the x and y directions respectively, and

$$\Lambda^+ = 0.5\left(\Lambda + |\Lambda|\right)$$

$$\Lambda^- = 0.5\left(\Lambda - |\Lambda|\right) \tag{3.5}$$

Combining and rearranging terms in the equations we get:

$$0 = \frac{\partial Q}{\partial t} + A^+\frac{\partial Q}{\partial \xi} + A^-\frac{\partial Q}{\partial \xi} + B^+\frac{\partial Q}{\partial \eta} + B^-\frac{\partial Q}{\partial \eta}$$

$$0 = \frac{\partial Q}{\partial t} + \frac{\partial F^+}{\partial \xi} + \frac{\partial F^-}{\partial \xi} + \frac{\partial G^+}{\partial \eta} + \frac{\partial G^-}{\partial \eta} \tag{3.6}$$

Now the flux vectors F^+, F^- and G^+, G^- are fluxes of positive and negative running characteristics. One physically correct differencing of the positive and negative running waves is to upwind difference the waves:

$$\Delta_t Q = -\Delta_\xi F^- - \nabla_\xi F^+ - \Delta_\eta G^- - \nabla_\eta G^+ \tag{3.7}$$

where $\Delta_\xi Z = Z_{i+1,j} - Z_{i,j}$ is a forward difference and $\nabla_\xi Z = Z_{i,j} - Z_{i-1,j}$ is a backward difference.

In order to have an upwind scheme appropriate to the running wave characteristic directions, a switching operator is needed. This operator is evaluated at $1/2$ points and selects values from j or $j+1$ points according to the characteristic direction of the waves. To obtain such a switching operator, we manipulate the equation futher. For simplicity, we discuss only the x-direction terms, since the y direction terms follow the same procedure. Now we have that

$$\Delta \tilde{Q} = -\bar{\delta}_\xi \tilde{F} - \bar{\delta}_\eta \tilde{G} \tag{3.8}$$

where

$$\bar{\delta}_\xi \tilde{F} = \tilde{F}_{i+\frac{1}{2},j} - \tilde{F}_{i-\frac{1}{2},j}$$

and

$$\tilde{F}_{i+\frac{1}{2},j} = \frac{1}{2}\left[F_{i+1,j} + F_{i,j} + (X_A \Phi_A)_{i+\frac{1}{2},j}\right] \tag{3.9}$$

The dissipation operators Φ_A are defined as follows:

$$(\Phi_A)_{i+\frac{1}{2},j} = g_{i,j} + g_{i+1,j} - \Psi\left(\lambda_{i+\frac{1}{2},j} + \gamma_{i+\frac{1}{2},j}\right)\alpha_{i+\frac{1}{2},j}$$

where

$$\alpha_{i+\frac{1}{2},j} = (X_A)^{-1}_{i+\frac{1}{2},j}\left[\frac{(JQ)_{i+1,j} - (JQ)_{i,j}}{\frac{1}{2}(J_{i+1,j} + J_{i,j})}\right]$$
$$\Psi(z) = |z| \tag{3.10}$$

and λ is an eigenvalue and X is the matrix of the right eigenvectors (X^{-1} is its inverse) of the flux Jacobian matrix defined by $A = \frac{\partial F}{\partial Q}$. Expressions for these terms can be found in many references on the subject [18, 19]. Φ is the dissipation term which will reduce the scheme to a first-order upwind at steep gradients, and Ψ is often called the coefficient of numerical viscosity. Finally,

$$g_{i,j} = S \cdot max\left[0, min\left(\sigma_{i+\frac{1}{2},j}|\alpha_{i+\frac{1}{2},j}|, S \cdot \sigma_{i-\frac{1}{2},j}\alpha_{i-\frac{1}{2},j}\right)\right]$$

$$S = sign\left(\alpha_{i+\frac{1}{2},j}\right)$$

$$\sigma \equiv \sigma(\lambda) = \frac{1}{2}\left(|\lambda| + \Delta t\lambda^2\right)$$

and

$$\gamma_{i+\frac{1}{2},j} = \begin{cases} \frac{(g_{i+1,j} - g_{i,j})}{\alpha_{i+\frac{1}{2},j}} & \text{if } \alpha_{i+\frac{1}{2},j} \neq 0 \\ 0 & \text{if } \alpha_{i+\frac{1}{2},j} = 0 \end{cases} \tag{3.11}$$

This scheme is theoretically second-order in space. A simple explanation of how the scheme works can be generalized as follows. This scheme can be viewed as a central-difference scheme where, for smooth regions, the dissipation term is turned off, giving $\Phi = 0$ so that,

$$\bar{\delta}_\xi \tilde{F} = F_{i+1,j} - F_{i-1,j} \tag{3.12}$$

which is a second-order central-difference scheme. On the other hand, for regions with steep gradient, then $\Phi \neq 0$, and

$$\tilde{F} = F_{i+1,j} \qquad or \qquad F_{i,j}$$

so that,

$$\bar{\delta}_\xi \tilde{F} = F_{i+1,j} - F_{i,j} \qquad or \qquad = F_{i,j} - F_{i-1,j} \tag{3.13}$$

which is a first-order upwind scheme.

3.2 Numerical Fluxes and Averaging

To evaluate the fluxes as desribed in the previous section, more terms need to be evaluated at the half points. First, the terms needed are presented here, then the procedure to extrapolate values to half points is described.

The eigenvalues, Λ, are given by:

$$\Lambda = \begin{bmatrix} U & 0 & 0 & 0 \\ 0 & U & 0 & 0 \\ 0 & 0 & U + c\sqrt{\xi_x{}^2 + \xi_y{}^2} & 0 \\ 0 & 0 & 0 & U - c\sqrt{\xi_x{}^2 + \xi_y{}^2} \end{bmatrix} \tag{3.14}$$

where U is the ξ-direction contravariant velocity, and c is the local sonic speed. The eigenvalues for the η direction are found by replacing U with V in the equations above, and ξ with η.

Now $\alpha_A = (X_A)_{i+\frac{1}{2}}{}^{-1} \Delta\tilde{Q}_{i+\frac{1}{2}}$ of Equation 3.10 can be written using:

$$\alpha(1) = \Delta\rho + \left(\frac{\gamma - 1}{c^2}\right) a_1$$

$$\alpha(2) = \frac{\tilde{\xi}_y}{\rho}(\Delta m - u\Delta\rho) - \frac{\tilde{\xi}_x}{\rho}(\Delta n - v\Delta\rho)$$

$$\alpha(3) = a_2 \left[\tilde{\xi}_x c(\Delta m - u\Delta\rho) + \tilde{\xi}_y c(\Delta n - v\Delta\rho) - (\gamma - 1) a_1\right]$$

$$\alpha(4) = -a_2 \left[\tilde{\xi}_x c(\Delta m - u\Delta\rho) + \tilde{\xi}_y c(\Delta n - v\Delta\rho) + (\gamma - 1) a_1\right] \tag{3.15}$$

where

$$a_1 = (u\Delta m + v\Delta n - \Delta e) - \frac{1}{2}\left(u^2 + v^2\right)\Delta\rho$$

$$a_2 = \frac{1}{\sqrt{2}\rho c}$$

$$\tilde{\xi}_x = \frac{\xi_x}{\sqrt{\xi_x{}^2 + \xi_y{}^2}}$$

$$\tilde{\xi}_y = \frac{\xi_y}{\sqrt{\xi_x{}^2 + \xi_y{}^2}}$$

To find the respective expressions in the η direction, η is substituted for ξ in the above equations. Variables expressed with Δ are defined as $\Delta Z = Z_{i+1,j} - Z_{i,j}$, but all other elements in Λ, X, and α are evaluated at half points (ie., $i + \frac{1}{2}$ or $j + \frac{1}{2}$ respectively).

To evaluate variables at half points, arithmetic averaging is used. This kind of averaging has the advantage of computational simplicity and can be extended for problems with chemical reactions. Other kinds of averaging can also be used, but they are usually more complicated and generally restricted to ideal-gas applications. Arithmatic averaging takes the form

$$\rho_{i+\frac{1}{2}} = \frac{1}{2}(\rho_{i+1} + \rho_i) \tag{3.16}$$

The same procedure is used to calculate u, v, U, V, ξ_x, ξ_y, η_x, and η_y, but for the speed of sound c, and $\tilde{\xi}_{i+\frac{1}{2}}$ and $\tilde{\eta}_{i+\frac{1}{2}}$, the following procedure is used:

$$c_{i+\frac{1}{2}} = \frac{1}{2}\left[H_{t,i+\frac{1}{2}} - \frac{1}{2}\left(u^2_{i+\frac{1}{2}} + v^2_{i+\frac{1}{2}}\right)\right] \tag{3.17}$$

$$\tilde{\xi}_{xi+\frac{1}{2}} = \frac{\xi_{xi+\frac{1}{2}}}{\sqrt{\xi_{xi+\frac{1}{2}}^2 + \xi_{yi+\frac{1}{2}}^2}} \tag{3.18}$$

where $H_{t,i}$ is the total enthalpy, defined by

$$H_{t,i} = \frac{\gamma p_i}{\rho(\gamma - 1)} + \frac{1}{2}\left(u_i^2 + v_i^2\right)$$

and $H_{t,i+\frac{1}{2}}$ is

$$H_{t,i+\frac{1}{2}} = \frac{1}{2}\left(H_{t,i+1} + H_{t,i}\right) \tag{3.19}$$

3.3 Time Discretization

Two time step methods were employed for the calculations of the present work. These were the Yoon and Jameson Lower-Upper Symmetric Gauss-Seidel (LU-SGS) scheme [20] , and an explicit scheme. The LU-SGS method was used to arrive at the steady state solutions, and the explicit method was used for the unsteady calculations. Because of the Courant number limitations on the explicit scheme very small time steps were necessary, and it was found to be prohibitively expensive computationally. Hence, the LU-SGS implicit scheme was used to accelerate convergence to the steady state solution since larger time steps can be used.

3.4 LU-SGS Implicit Scheme

The LU-SGS scheme used is described in detail elsewhere [20-22]. The advantage of the scheme is that it is implicit and large time steps can be used, and that no

block tridiagonal inversions need to be performed. As presented below it is 2nd order accurate in time, and for constant Δt can be written as:

$$LD^{-1}U\delta Q = -\Delta t R \tag{3.20}$$

where

$$L = I + \frac{\Delta t}{2}\left(\nabla_\xi A^+ + \nabla_\eta B^+ - A^- - B^- - \frac{\partial H}{\partial Q} + \frac{\partial W}{\partial Q}\right)$$

$$D = I + \frac{\Delta t}{2}\left(A^+ - A^- + B^+ + B^-\right)$$

$$U = I + \frac{\Delta t}{2}\left(\Delta_\xi A^- + \Delta_\eta B^- + A^+ + B^+\right)$$

$$R = \Delta_\xi F + \Delta_\eta G + H - W$$

Here the Jacobian matrices are constructed to give diagonal dominance, with

$$A^+ = \frac{1}{2}(A + r_A I); \qquad B^+ = \frac{1}{2}(B + r_B I)$$

$$A^- = \frac{1}{2}(A - r_A I); \qquad B^- = \frac{1}{2}(B - r_B I) \tag{3.21}$$

where

$$r_A = max\left(|\lambda_A|\right)$$

$$r_B = max\left(|\lambda_B|\right) \tag{3.22}$$

and where

$$\delta Q = Q^{n+1} - Q^n \tag{3.23}$$

3.5 Explicit Scheme

The explicit scheme used for the time accurate unsteady calculations is simply given as:

$$Q^{n+1} = Q^n - \Delta t(\Delta_\xi F + \Delta_\eta G + H - W) \tag{3.24}$$

Chapter 4

Computational Method

The ram accelerator problem is difficult to solve numerically. Because of the large gradients at the area discontinuity and the extremely large accelerations, special considerations must be made to ensure stability and reliability in the numerical results. The steep gradients can only be handled by using a zonal method, which is described in detail in a later section. In addition, the initial conditions must be carefully selected to ensure quick and reliable convergence. The solution method that is employed is described below, and the boundary and initial conditions are explained in detail. A description of the heat addition model is also provided.

4.1 Solution Method

Although the intent of this thesis is to provide a non-steady model for the ram accelerator projectile, calculations must start from a converged, steady state solution. This method is required, because without a combustion model and sabot interactions the problem cannot be solved otherwise. Once a steady state solution is achieved, the nonsteady terms can be activated, and the effects of acceleration,

determined by the heat release of the gas mixture, can be investigated. Because of the Courant number requirements for the explicit scheme, the time step used is very small (on the order of 0.1 μs). This requires that approximately 10000 iterations be performed per millisecond of physical time. This extremely small time step is dictated by the high velocity and small length scale of the problem. For this reason, to reach a steady state solution the LU-SGS scheme described in the previous chapter is used. Once the steady solution has been reached, then the explicit scheme is used to calculate the time accurate unsteady effects of the problem.

Since the code does not yet allow for sabot interactions, the initial starting transients cannot be modeled. Hence, the shock cannot be stabilized on to the projectile body by the pressure on the face of the sabot, and it must somehow be positioned there initially. Because of the nature of the heat addition model special attention must be paid to achieving the steady state solution.

There are several techniques of establishing the initial shock system on the body. A zero velocity outflow condition can be assumed, which effectively represents the face of the sabot. Once a normal shock is established, the forced boundary condition at the outflow is removed and the solution is allowed to reach steady state for the given heat release. This can be tricky, because often the amount of heat added is too great, in which case the diffuser unstarts. In addition, if the heat addition is too low, the wave falls off the rear of the projectile.

Another technique is to artificially establish the shock on the projectile. Again, the solution is allowed to reach steady state for the given heat release. The same problems arise in this technique as mentioned in the previous method. In

another method, a shock can be established by adding heat to the flow behind the projectile. This causes the pressure to rise, and a shock establishes itself at the base and moves forward on the projectile. This method is very time consuming since the velocity of the stream is supersonic and a substantial number of iterations are required to generate a stable solution. The consequences of this are discussed in Chapter 5.

4.2 Code Validation

Several test cases were used to validate the numerical results of the code. First, the code was validated on benchmark cases, and then was applied to specific ram accelerator cases. The latter test cases are discussed in the results section in the following chapter.

The ablility of the TVD scheme to capture shocks was tested by solving a shock reflection problem with a freestream Mach number of $M = 2.9$. The inflow and outflow conditions were assumed supersonic, and the wall boundary condition was free-slip inviscid. The upper boundary was initialized to the appropriate values for the problem. The computational domain was 61×21 in the x and y directions respectively. A very crisp shock was captured in only three grid points. This non-oscillatory and crisp shock capturing ability is essential in the numerical simulations of compressible flows, since unsteady shocks will be present.

The drag calculations on a supersonic projectile were tested using a 2D wedge and a symmetric diamond airfoil. The domain was 64×21 in the x and y directions respectively. The inflow and outflow were supersonic, the projectile surface was free-slip inviscid, and the upper boundary was direct extrapolation.

The freestream Mach number in both cases was 3.0. The results of the drag calculations in both cases agreed very well with predicted results using the Method of Characteristics [23].

The zone coupling was tested with a shock propagation problem. The domain was 32×21, and the inflow condition was supersonic. The outflow velocity was fixed to zero, and the upper and lower walls were free-slip inviscid. A shock was generated on the outflow surface by the boundary condition and was allowed to propogate upstream. The shock crossed the zone boundary with no anomalies or oscillations.

To test the ability of the numerical formulation to handle the steep gradients about a sudden expansion, and to further test the zone coupling region, supersonic flow over a rearward facing step was solved. Even though the present work solves the Euler equations, a recirculation region was captured. This is due to the numerical viscosity of the scheme being used. The terminating Mach line of the expansion was in good agreement with Prandtl-Meyer expansion theory [23].

4.3 Computational Domain

The computational domain selected for the current problem is shown in Figure 4.1. The y direction has been magnified by a factor of five for clarity. The throat diameter, nosecone angle, projectile length, and tube diameter can be easily varied through a grid generating program. Most of the calculations in this thesis have been performed on a nominal projectile with a nosecone half-angle of 10 degrees, a throat diameter of 28.9 mm, and a projectile body length of 84 mm. The base diameter of the projectile is calculated by using the blockage area of the actual

projectile, including the fins. An effective base diameter is then calculated, which for this case corresponds to 22.6 mm. The tube diameter is 38 mm.

The grid itself is algebraic, as the problem domain is not overly complex to justify an elliptic solver. It is separated into two zones to facilitate capturing of the expansion region at the rear of the projectile. If a single zone is used the gradients are too steep and the code does not give solutions.

Zone 1 is 164×21 and Zone 2 is 77×22. The length of the region behind the projectile is required for the heat addition model. There is evidence to indicate that heat is added over one projectile length behind the body. This is discussed in more detail in the following section. The grids overlap by one line of points through which information is passed.

4.4 Heat Addition Model

The method of heat addition chosen, and the region over which heat is added, can drastically affect the transient pressure profiles and the convergence rate. It was found that the steady state result with heat addition was independent of the region of heat addition (as would be expected), but that the unsteady pressure profiles were affected by the heat addition model. Therefore, even though the model selected was found to require substantially more iterations to achieve a steady profile, in order to attempt to model the unsteady phenomena the heat addition region of Figure 4.2 was selected.

There is evidence to indicate that heat addition occurs over a region that extends up to one projectile length behind the body [24]. The particular heat release region of Figure 4.2 was selected in order to match the actual physics of the

combustion region behind a dump combustor or flame- holder, as shown in Figure 4.3. The gases behind the bluff body are fully combusted, and the flame-spreading angle varies between 2-8 degrees [25].

The amount of heat added is arbitrarily chosen to be between the upper limit of the maximum available heat assuming complete combustion of the gases entering the control volume, and the heat release associated with a Chapman-Jouget wave. The heat is added in the region shown, and if it is insufficient to establish a wave on the projectile given certain operating conditions, then it is increased until a shock can be stabilized on the projectile. This amount of heat is then used to perform the calculations. If the heat release is too great, then the upstream conditions change to the point where an unstart situation ocurrs, and the heat added must be decreased.

4.5 Initial Conditions

Because the final solution is actually reached through a progression of previous results, several different initial conditions need to be addressed. First, a steady state supersonic profile is generated over the projectile which is then used as the starting point for the heat addition calculations. A steady state condition is then reached for a given heat release which stabilizes the shock location on the projectile. Once this condition has been achieved, the projectile is allowed to accelerate and the unsteady effects of the problem can be observed. In addition, the heat release can be varied at any time throughout the process to see the effects of heat release in different regions of the flow, including on the projectile body.

The initial conditions to generate the steady state supersonic profiles are

described here. Zone 1 is initialized to freestream conditions, which for the present case are a freestream velocity corresponding to a Mach number of $M_\infty = 3.21$, a tube fill pressure of 25 atm, and the corresponding gas properties of the nominal first stage mixture, $2.7CH_4+2O_2+5.8N_2$. Zone 2 is initialized to freestream density and pressure, but to a velocity in the x direction of $U = \frac{U_\infty}{4}$ and to a velocity in the y direction of $V = \frac{-U_\infty}{16}$. These particular conditions were found to help accelerate convergence to the steady state supersonic profile. This particular freestream Mach number was chosen so that the numerical results could be compared to available experimental results.

The initial conditions for the case with heat addition are for the same gas mixture above, but for a freestream velocity corresponding to $M_\infty = 2.98$. The pressure and density are the same. Again, the freestream Mach number was selected in order to compare numerical results with available experimental results. Once the supersonic profile is achieved, heat is added to the flow to establish the shock system on the projectile. The initial conditions for this calculation are just the flow field solutions of the supersonic profile. The initial conditions for the final unsteady calculations are the steady state solutions with heat release.

4.6 Boundary Conditions

For Zone 1 the inflow ahead of the projectile is supersonic, hence all the flow variables are known and do not change. The outflow conditions may vary from supersonic in the case of no heat addition, to sonic or subsonic for the case of thermal choking at the exit, to supersonic for the case of choking and supersonic expansion. In the case of supersonic outflow, direct extrapolation is used and

$Q_{imax} = Q_{imax-1}$. For subsonic outflow, the local Rieman invariants at $i = imax-1$ are used to back out the correct flow properties at $i = imax$. These are given in generalized curvilinear coordinates as:

$$R_1 = V_n + \frac{2c}{\gamma - 1}$$

$$R_2 = R_1 - \frac{4c}{\gamma - 1}$$

$$S = \frac{\rho^\gamma}{p}$$

$$R_4 = V_t \tag{4.1}$$

Here c is the local speed of sound given by $c = \sqrt{\frac{\gamma p}{\rho}}$, and S is the entropy. The velocities V_n and V_t are the normal and tangential velocities to a $\xi = constant$ line. They are given by:

$$V_n = \frac{\xi_x u + \xi_y v}{\sqrt{\xi_x{}^2 + \xi_y{}^2}}$$

$$V_t = \frac{\xi_y u - \xi_x v}{\sqrt{\xi_x{}^2 + \xi_y{}^2}} \tag{4.2}$$

The projectile surface itself is assumed to be solid wall and inviscid. The velocity components at the wall where $\eta = constant$ are given by Equation 4.2 with η substituted for ξ. Then

$$\begin{pmatrix} u \\ v \end{pmatrix} = \frac{1}{\sqrt{\xi_x{}^2 + \xi_y{}^2}} \begin{bmatrix} \eta_y & \eta_x \\ -\eta_x & \eta_y \end{bmatrix} \begin{pmatrix} V_t \\ V_n \end{pmatrix} \tag{4.3}$$

Here we specify that $V_n = 0$, and V_t is obtained by direct extrapolation from the interior. The pressure is then obtained by solving the normal momentum equation at the wall. In curvilinear coordinates this can be given as:

$$\left(\eta_x \xi_x + \xi_y \eta_y\right) p_\xi + \left(\eta_x{}^2 + \eta_y{}^2\right) p_\eta = -\rho U \left(\eta_x u_\xi + \eta_y v_\xi\right) \tag{4.4}$$

The ξ derivatives are centered differenced and the η derivatives are first order one sided differenced. The wall itself is assumed to be adiabatic, which implies that total enthalpy is conserved. The upper boundary representing the tube wall is modelled as a free-slip boundary, where the flow properties are extrapolated from the interior, and the velocity in the y direction is $v_{jmax} = -v_{jmax-1}$.

For Zone 2 the left boundary is a solid wall, and the normal momentum equation is solved at the surface. This is similar to Equations 4.4 with the appropriate substitutions for ξ and η. The outflow boundary is identical to the outflow boundary conditions for Zone 1. The lower surface, representing the slip line of the axisymmetric problem, is a free-slip inviscid condition with $v_{jmin} = -v_{jmin+1}$. The upper surface is the zone coupling interface with Zone 1.

The interface between the two zones is treated by directly passing the information between the overlapping grid points. Once the updated solution is calculated for the lower surface of Zone 1, it is passed directly as the upper boundary condition to Zone 2. Similarly, the updated solution of Zone 2 is then passed directly to the lower boundary of Zone 1. The solution alternates between zones.

The boundary conditions used in the computations are summarized in Figure 4.4.

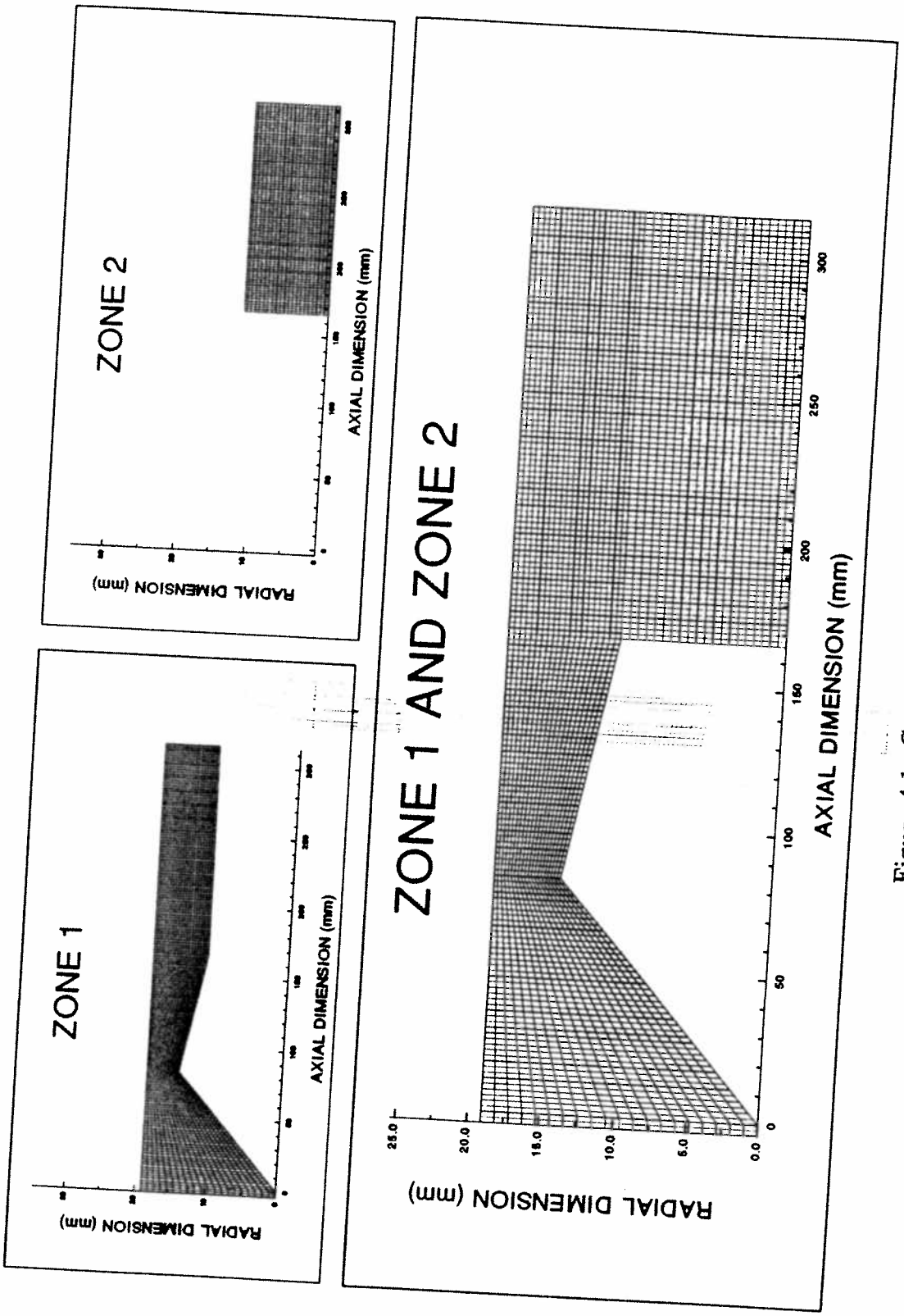

Figure 4.1: Computational Domain

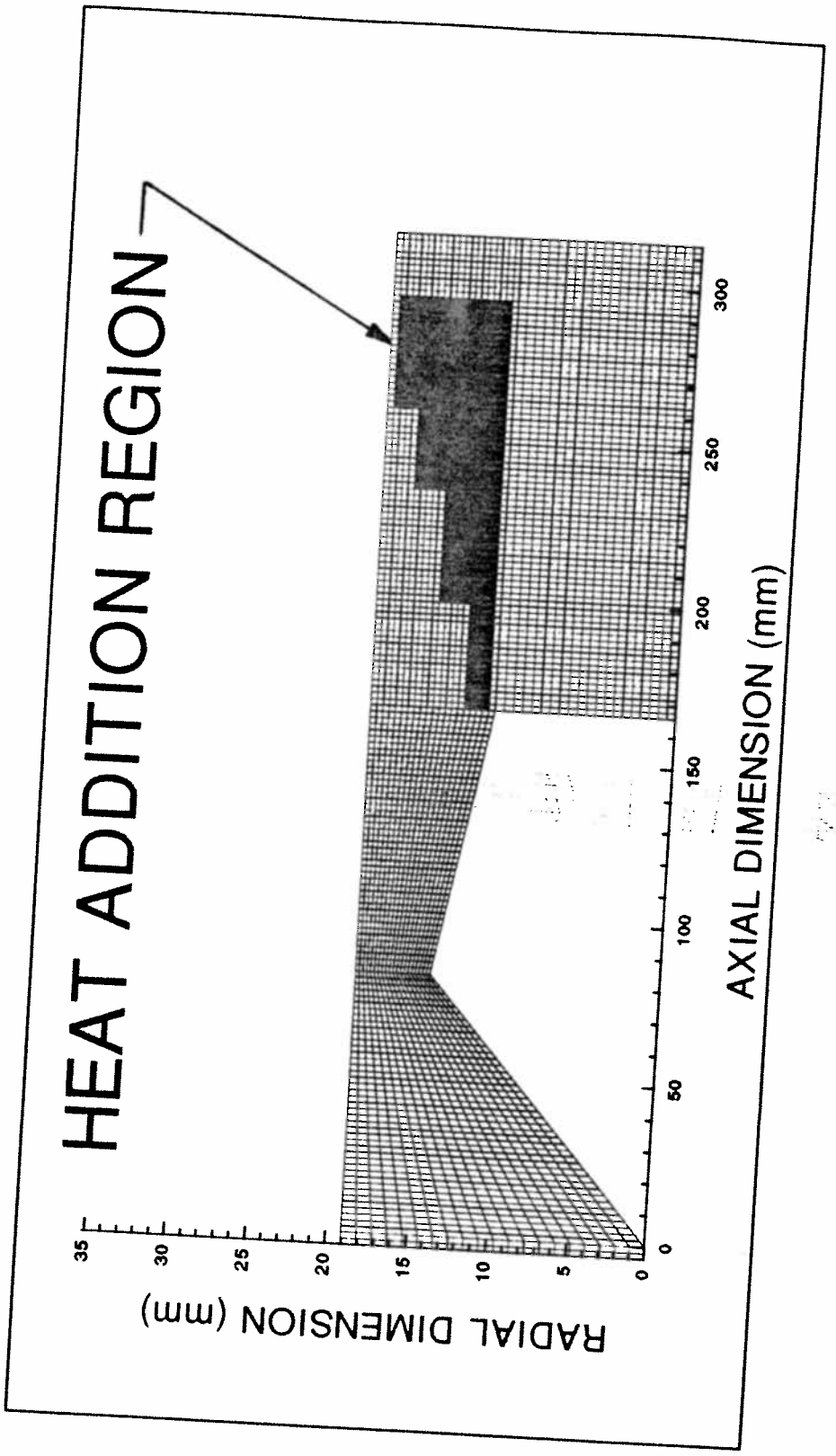

Figure 4.2: Heat Release Region for Current Study

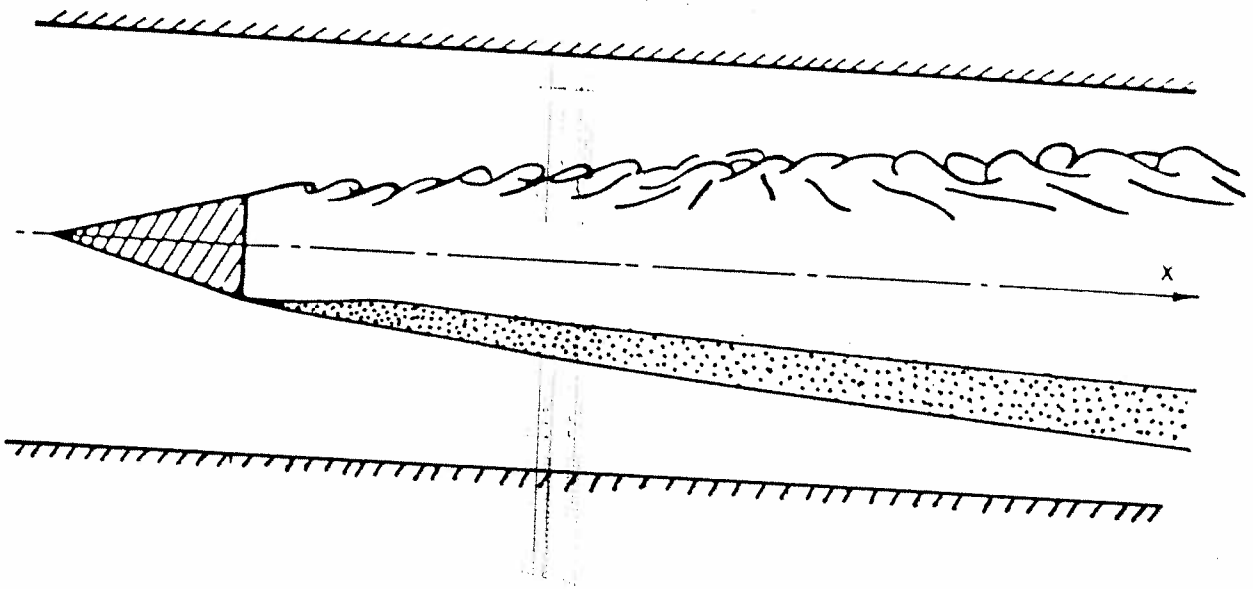

Figure 4.3: Heat Release Region of Bluff Body Flameholder [25]

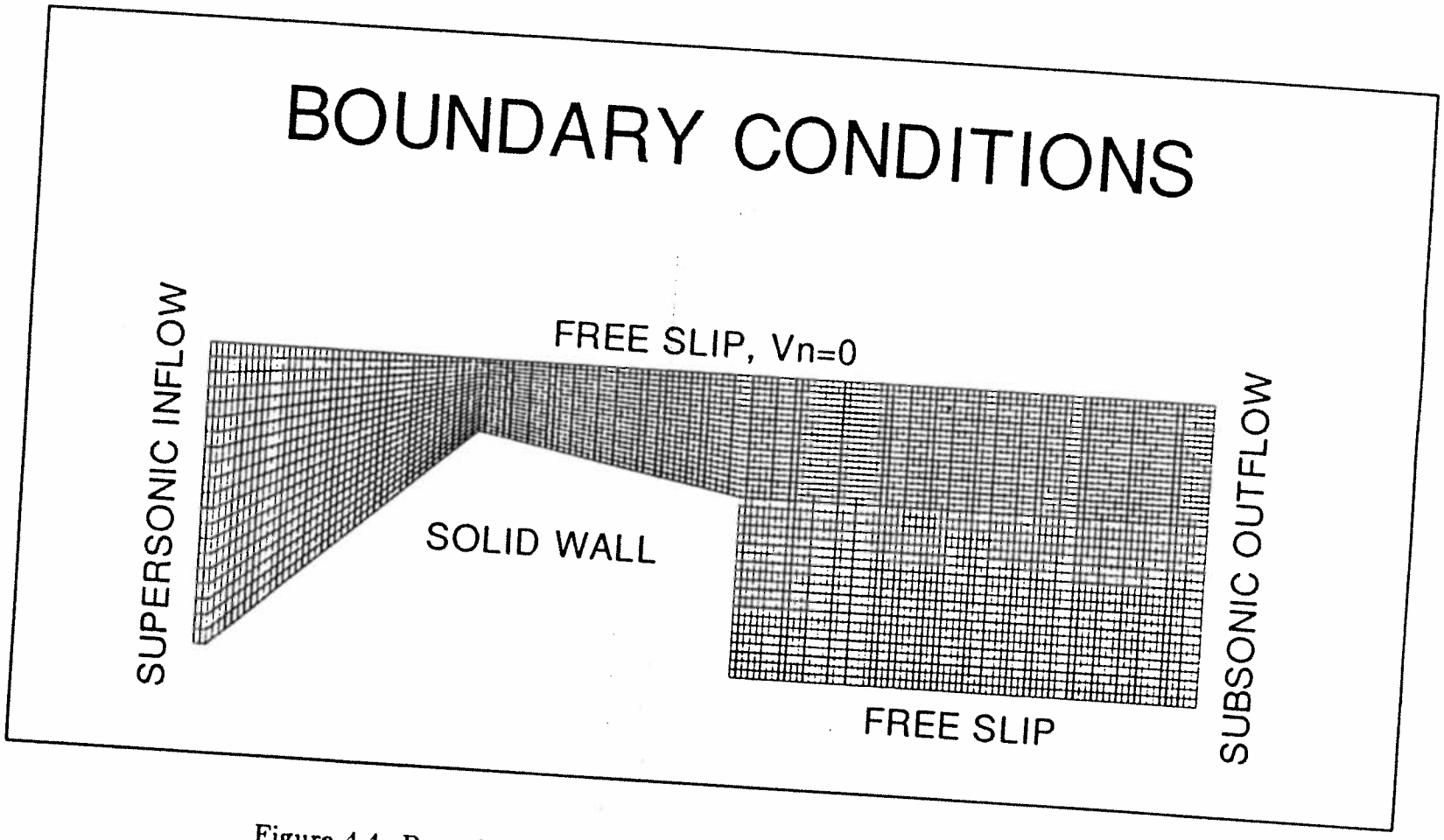

Figure 4.4: Boundary Conditions for Zone 1 and Zone 2

Chapter 5

Results and Discussion

Several different types of calculations were performed for the ram accelerator projectile configuration. These included supersonic profiles, steady state heat addition, and unsteady calculations for an accelerating projectile.

All the present calculations have been performed for a nominal first stage mixture of $2.7CH_4 + 2O_2 + 5.8N_2$. This particular mixture has a speed of sound $c = 363$ m/sec, a maximum heat release of $\Delta H = 76.45$ kJ/mole assuming complete combustion, and is initially at a freestream temperature of $T = 300$ K and a fill pressure of 25 atm. The results in this mixture are qualitatively similar to all others. The 1st stage has been chosen for this study because it is the most extensively studied experimentally and many data are available for comparison to the numerical calculations. The results are representative of the code's ability to accurately model the subsonic combustion thermally choked ram accelerator mode, and other gas mixtures can be solved for as desired.

The projectile configuration is detailed in the Chapter 4, but briefly it has a 28.9 mm throat diameter, a 10 degree half-angle nose cone, a body length of 83.8 mm, and a base diameter of 22.6 mm. The body length does not include

the length of the nosecone. The tube diameter is 38 mm.

In all the figures of this chapter, the y axis has been magnified by a factor of five for clarity and the projectile extends from $x = 0$ to $x = 166$ mm. The projectile throat is at $x = 82$ mm. All the current calculations were performed for the grid described in Chapter 4. Several calculations were performed for a finer grid, where Zone 1 was 196×21 and Zone 2 was 109×31, but the results did not change, and the added expense computationally was not warranted for this particular case. The advantage of a coarser grid is faster convergence, since fewer calculations are required.

5.1 Supersonic Profiles with no Heat Addition

Several cases were run to test the code's ability to correctly model the supersonic flow about the projectile without combustion. Figure 5.1 shows a series of pressure contours for a situation where the freestream velocity is not sufficient to start the diffuser. A shock can be seen to be generated at the throat where the flow chokes (ie. goes to $M = 1$), and then propagates forward in a classical Kantrowitz unstart. The subsonic pressure profile at the tube wall for the case of Figure 5.1 (c) is shown in Figure 5.2, and is compared to experiment in Figure 5.3. The pressure jump represents the normal shock ahead of the projectile, and the drop in pressure is due to the subsonic flow over the projectile choking at the throat and then expanding supersonically over the body. The second pressure drop represents the expansion over the base of the projectile at the discontinuous area change. The computed peak pressure is 218 atm. It was determined that the computed minimum starting Mach number for this particular throat diameter was $M = 2.73$,

and this is in excellent agreement with the experimental minimum of $M = 2.7$.

When the minimum starting Mach number is exceeded, then the supersonic pressure contours of Figure 5.4 result. The oblique shocks through the diffuser are crisply captured by the TVD scheme. The expansion region about the base of the projectile is clearly visible, and the recompression shock created by the turning of the flow after the recirculation region can be made out. The streamlines are shown in Figure 5.5. It should be noted that the base flow region is not a true recirculation region. Rather, it represents the area behind the terminating Mach line of a Prandtl-Meyer expansion. The circulation within this region is caused by numerical viscosity and artificial dissipation, and hence is strictly a result of the numerics.

The pressure profile along the tube wall is shown in Figure 5.6, and is compared to the experimental results of Figure 5.7. The first pressure peaks represent the conical shock reflections in the diffuser; the pressure then drops across the base expansion, and the subsequent peaks represent the recompression shocks. Numerically the peak pressure was determined to be 153 atm, which is in good agreement with the experimental results of 165 atm.

Once the steady state profile is obtained the projectile is allowed to undergo acceleration. In the case of no heat addition the pressure and wave drag on the projectile result in deceleration and velocity profiles which are substantially lower than the experimental values (the deceleration is only 0.25 of what is observed experimentally). This may be attributed to the fact that the numerical model does not take into account the pressure and wave drag of the fins which exist in the experiments, nor does it account for the friction drag of the fins on the

tube wall. Given the high accelerations of a thrusting projectile, these effects are assumed to be negligible for those cases. The decceleration decreases as the projectile slows, as is expected. Eventually the Mach number at the throat reaches unity, and the shock is propagated ahead of the projectile in a Kantrowitz unstart fashion.

5.2 Ram Accelerator with Heat Addition

5.2.1 Steady Calculations

The results of the ram accelerator projectile configuration with heat addition are discussed here. Figure 5.8 shows a pressure contour plot of a steady state case. Here steady state is taken to be when the force acting on the projectile does not change more than 1.5×10^5 between iterations. It is evident that a normal shock exists on the projectile body for a given heat release. In an actual experiment the shock system is suspected to be a complex series of oblique and normal shocks due to the presence of the fins and shock/boundary layer interactions. The amount of heat added in this particular case is 0.55 of the total available heat of the gas entering the control volume, assuming complete combustion. For this amount of heat it is shown that the shock is pushed well forward on the projectile. It should be noted that depending on the amount of heat released behind the projectile, the normal shock may not be able to push onto the projectile, or that it may overshoot the projectile in an unstart situation. The Mach contours are shown in Figure 5.9. The choke point, $(M = 1)$, is located at the end of the heat addition zone. There is supersonic expansion behind this region. It should be noted that the transient pressure profiles that lead to the establishment of the shock on the

projectile can vary dramatically for different models of the heat release region. For example, for a case where the heat was added over a rectangular region at the base of the projectile instead of the current stair-step method, the shock was formed immediately on the base of the projectile and moved up rapidly to its steady state position. For the stair-step heat addition the pressure waves formed by the different regions of the heat addition zone had to coalesce before they could form the shock and move up onto the projectile. This resulted in substantially different transient profile.

It was found that for a heat release of 0.55 of the total available heat the shock could barely be established on the base of the projectile. However, if the shock was forced onto the projectile and the same amount of heat was added, then the heat was sufficient to keep the normal shock well on the body. This is due to the discontinuous area change at the base. If the projectile were tapered to a point the pressure waves would encounter less resistance and could push the shock more readily onto the body. This implies that for a projectile with a discontinuous area change the initial outflow boundary conditions are essential for helping establish the shock system on the projectile. Credence is given to this result by the fact that no experiments have been conducted where a wave that has fallen off the projectile could be pushed back onto it. What is seen experimentally is that the wave behind the projectile develops into a C-J detonation wave which overtakes the projectile and creates an unstart. A wave with the heat release of a C-J wave has sufficient strength to overcome the discontinuous area change, however, once on the projectile its heat release is too high and the flow chokes on the body which leads to an unstart.

The pressure profile on the tube wall is shown in Figure 5.10, and is compared to the experimental results of Figure 5.11. Although the pressures are qualitatively similar, no direct comparison can be made because of the arbitrariness of the heat addition in the numerical model. If the right amount of heat is selectively added, then the profiles can be made to agree almost exactly. If the thrust is matched, then the peak pressures are of the same amplitude and are in excellent agreement. There is a jump in pressure due to the normal shock, and then a gradual rise to the peak pressure. The peak pressure in the numerical model ocurrs at the point where the heat addition begins, at the base of the projectile.

5.2.2 Unsteady Calculations

Once steady flow has been achieved the projectile is allowed to undergo acceleration with a constant percentage of the total amount of heat available being added to the flow. The velocity profile of this calculation is shown in Figure 5.12, and is compared with experiment and quasi-steady theory on the same figure. The solid squares represent the experimental values and the dotted curve represents the quasi-steady theory. The computational results are the solid line. Deviation from steady theory is discussed later in this section. As the velocity of the projectile increases the wave moves further back along the body and the acceleration decreases. For this heat release the wave can be sustained at the base of the projectile, but its strength is considerably weakened.

The Mach contours that result in this situation are very interesting, and are shown in Figure 5.13. The shock, which is no longer normal, is not sufficiently strong to render the flow behind it subsonic over its entire range. This results in

a mixed flow situation, where part of the heat is being added supersonically and part of the heat is being added subsonically, at least for the current heat release model. As the projectile continues to accelerate, the supersonic region increases in size. Throughout this whole time, even though the thrust is decreasing, there is still a net forward thrust that is quite substantial. The particular effects of supersonic heat addition are not investigated further at this time.

As the projectile accelerates, the velocity and acceleration are lower than that predicted by quasi-steady theory for a given heat release. Indeed, if the heat added as a percentage of the total available heat is not appropriately increased for the unsteady case, then the wave recedes on the body, and it may eventually fall off the projectile if the heat added is not sufficiently high. Hence, a higher heat addition is required for the unsteady case than for the quasi-steady case to produce the same acceleration.

The effects of unsteadiness are to decrease the thrust relative to the steady case for a given heat release. If this is the case, then it implies that in order to maintain the increasing thrust seen in the experiments, proportionally more heat must be added in the quasi-steady model as the projectile accelerates. In the unsteady case, however, work is performed by the flow in accelerating the vehicle. This work is removed from the flow, and its total temperature is therefore decreased. This reduction in total temperature subsequently allows proportionally more heat to be added to the flow, resulting in a greater thrust. This can explain the good agreement of the unsteady model with the experimental results at the higher velocity ranges. The higher the velocity, the more important the unsteady effects become.

In addition, it should be noted that the amount of heat that can be added to the unsteady problem can greatly exceed the amount of heat that would cause an unstart in the steady case at the same operating conditions. Hence, when modelling the higher velocity ranges of the thermally choked propulsion mode the unsteady effects are critical. A greater total heat release in an unsteady problem could explain the high thrust seen experimentally that deviates from the quasi-steady model, which predicts an unstart for the same amount of heat release. This implies that the important parameter for predicting the acceleration at the upper velocity range is the total heat that is being added to the flow, and that as this continues to increase the net thrust on the projectile also increases. Hence, in theory, the heat added can be increased beyond the point required to accelerate the projectile to the C-J velocity of the mixture without causing an unstart for the unsteady case. There can then be a smooth and continuous transition between the subdetonative and superdetonative velocity ranges, since the diffuser will not unstart for the greater heat release.

If the projectile accelerates to the point where the heat release is no longer sufficient to maintain the shock on the body, wave fall-off can occur. It should be noted that the same amount of heat that results in a fall-off on a blunt based projectile for the unsteady case is sufficient to maintain the shock on the body at the velocity where fall-off ocurrs if the problem were solved in steady state. If, on the other hand, too much heat is added to the unsteady flow, the normal shock overtakes the projectile and an unstart ocurrs.

It should be noted that if the heat release region used is the stair-step model, in order to cause an unstart for the unsteady calculations, and sometimes

in order to maintain the shock on the projectile at the higher velocity ranges (i.e. higher than 1580 m/sec), the heat added must exceed the maximum heat available in the flow. This implies that experimentally the heat is released in a different region of the flow than is being modelled here. It was found that if the same amount of heat is added to the flow, but is distributed in a way that includes heat addition on the projectile, then the unsteady case could result in an unstart for what would normally be a valid operating region. If we redistribute the total amount of heat that resulted in a previously stable configuration partially onto the body, it can be shown that the projectile quickly unstarts. Hence, the movement of the heat addition region is also critical for predicting the performance of the ram accelerator in the upper velocity range, at least for the unsteady case. For the steady case the location of the heat addition region would make no difference in the shock location or the thrust.

Figure 5.1: Pressure Contours for Vehicle Below Minimum Starting Velocity

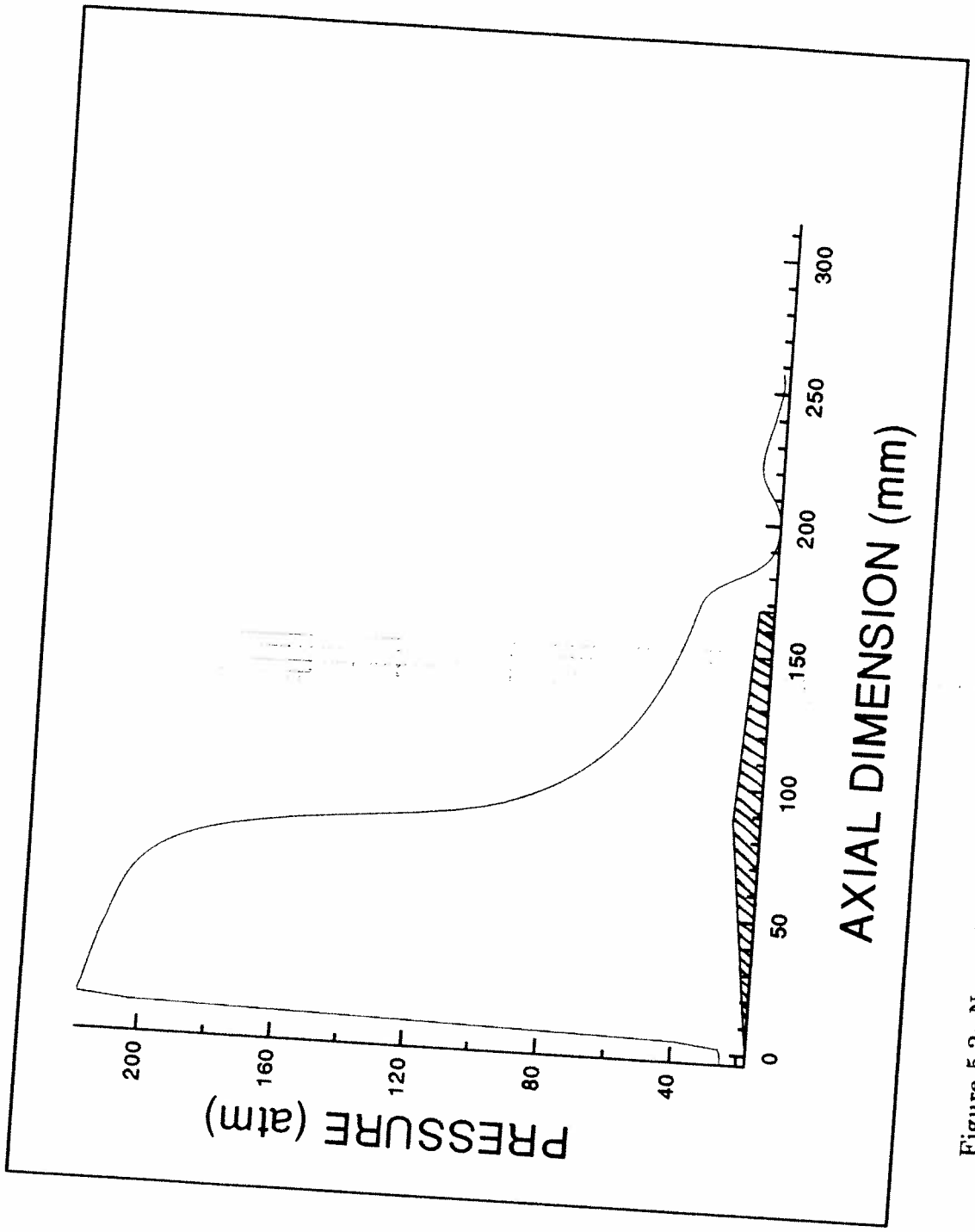

Figure 5.2: Numerical Pressure Profile at Tube Wall for Vehicle in Subsonic Flow

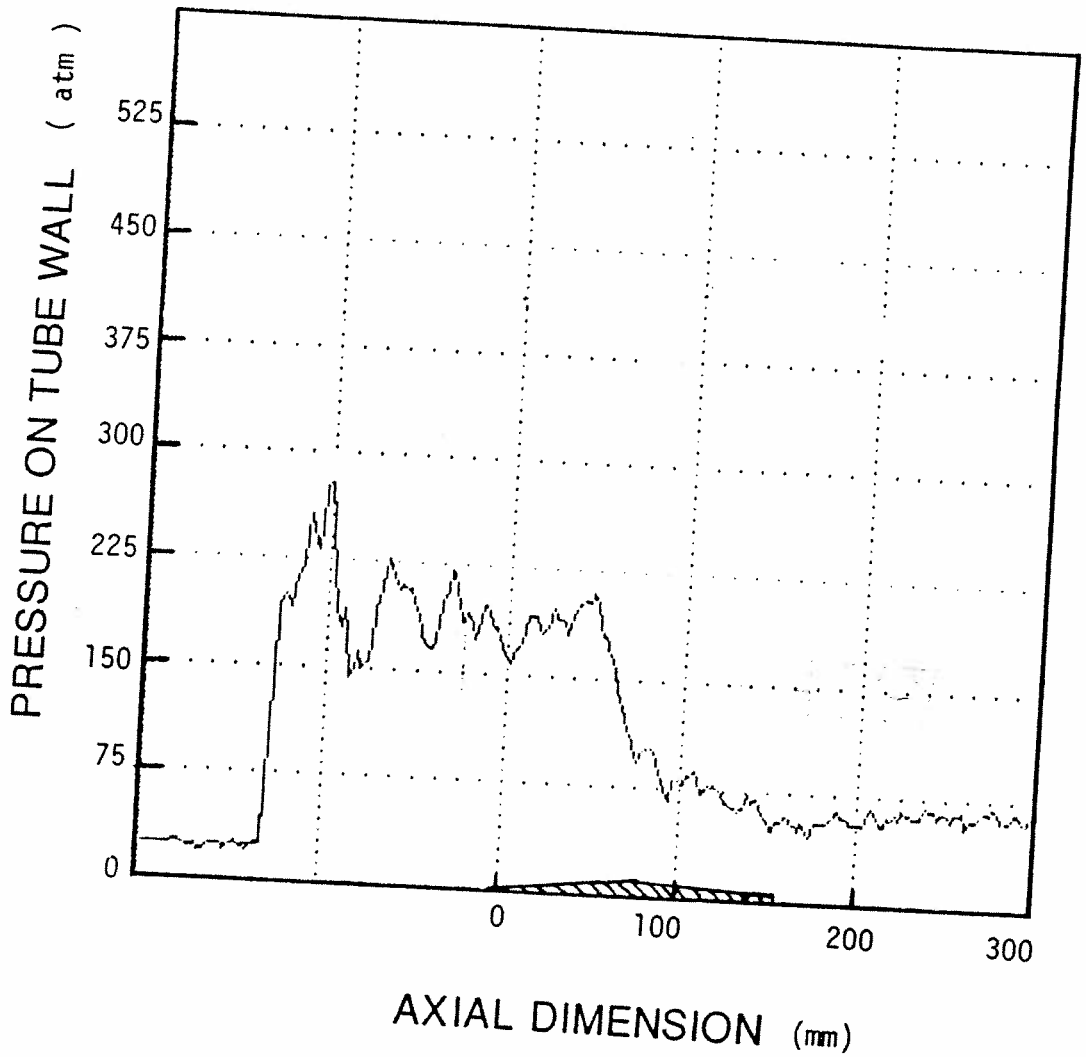

Figure 5.3: Experimental Pressure Profile at Tube Wall for Vehicle in Subsonic Flow

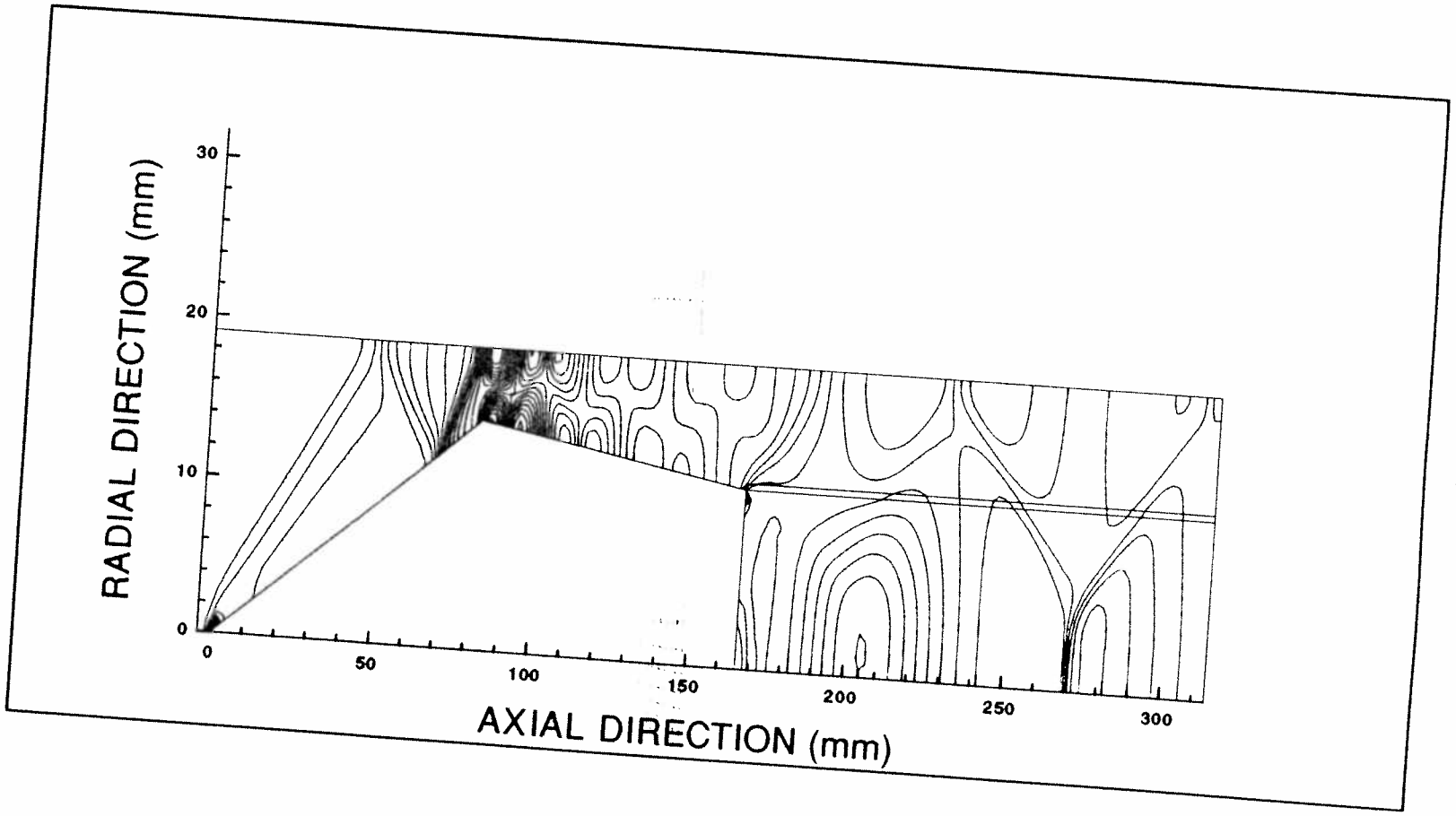

Figure 5.4: Pressure Contours for Vehicle in Supersonic Flow (No heat addition)

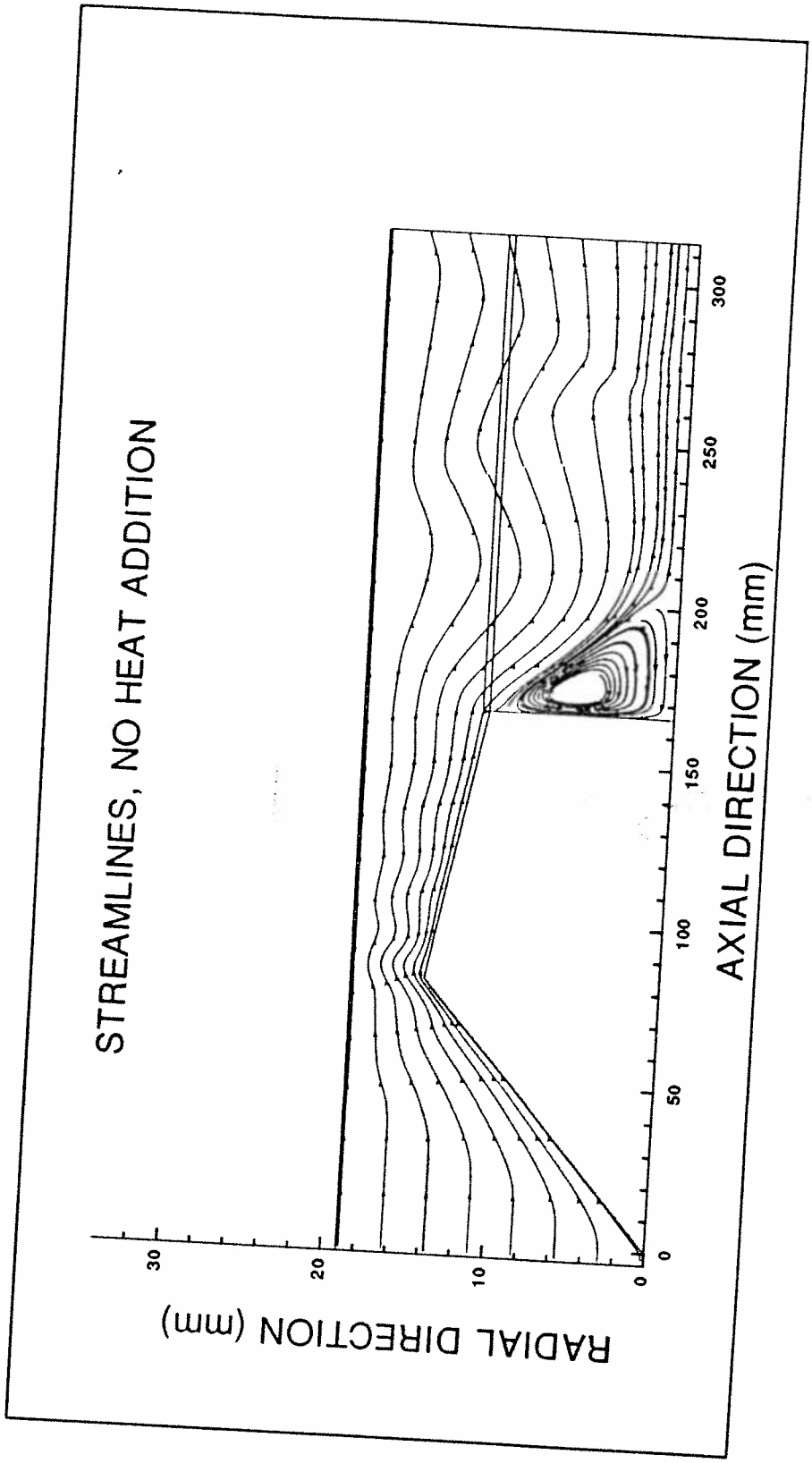

Figure 5.5: Streamlines for Vehicle in Supersonic Flow (No heat addition)

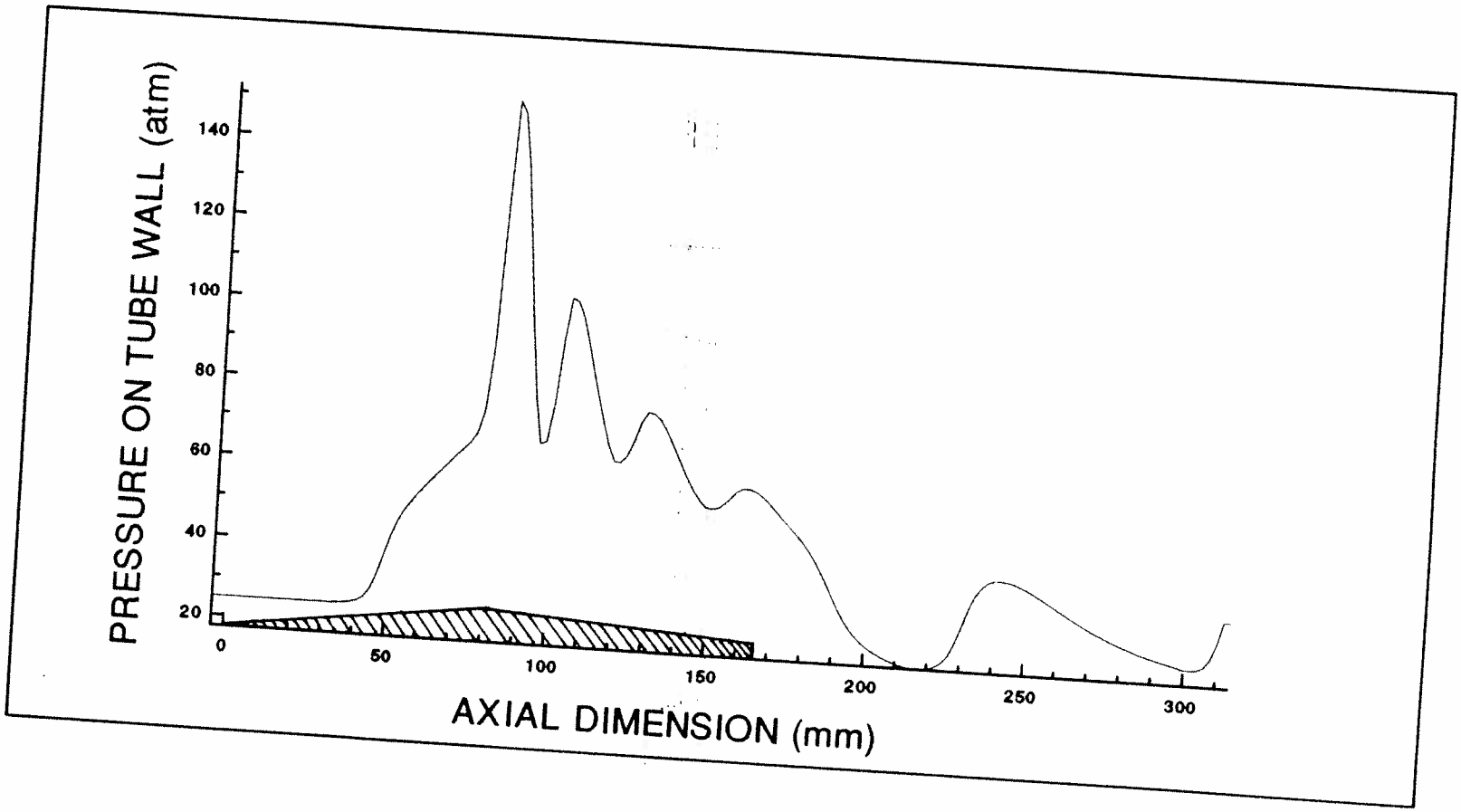

Figure 5.6: Numerical Pressure Profile at Tube Wall for Vehicle in Supersonic Flow

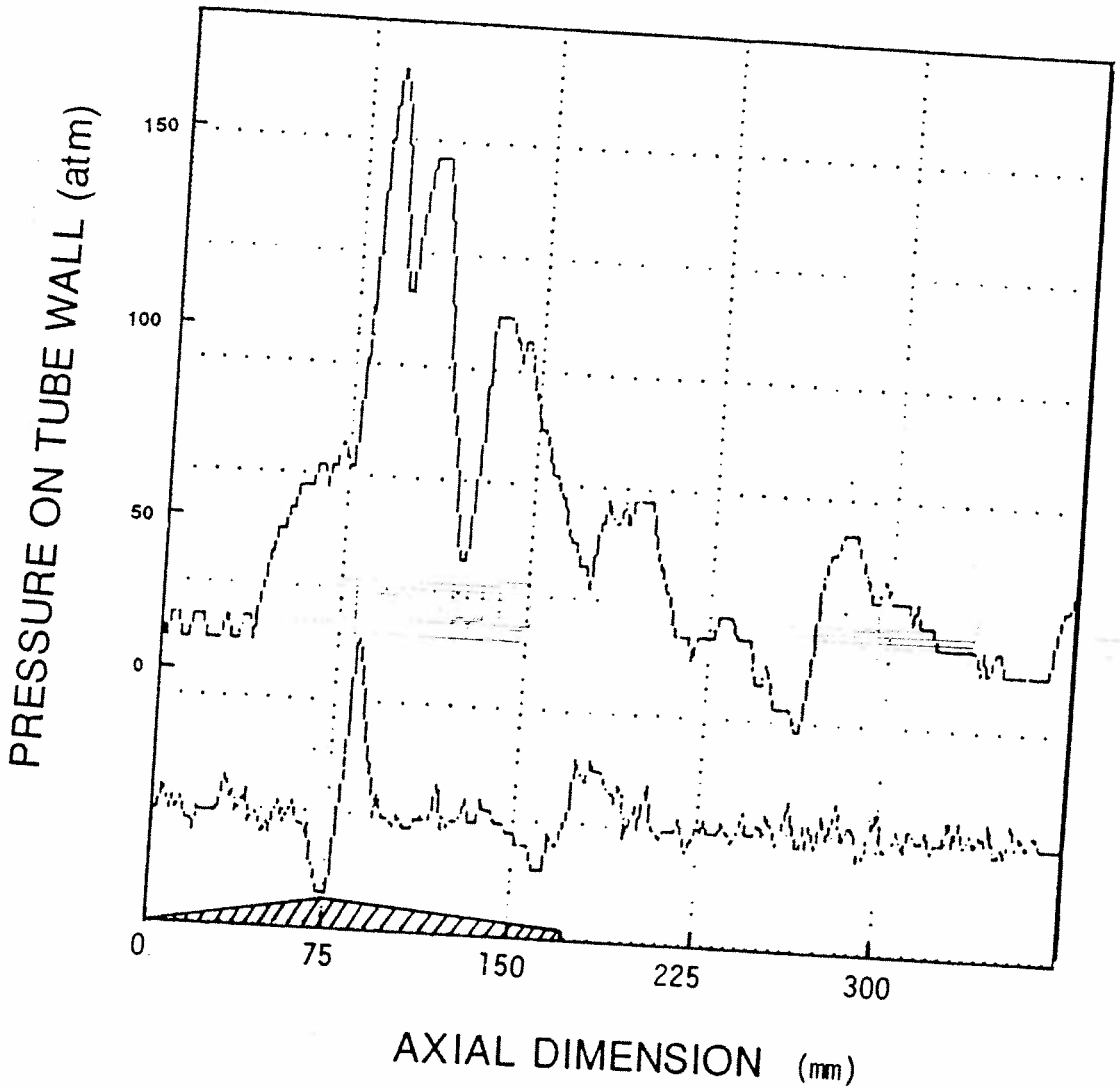

Figure 5.7: Experimental Pressure Profile at Tube Wall for Vehicle in Supersonic Flow

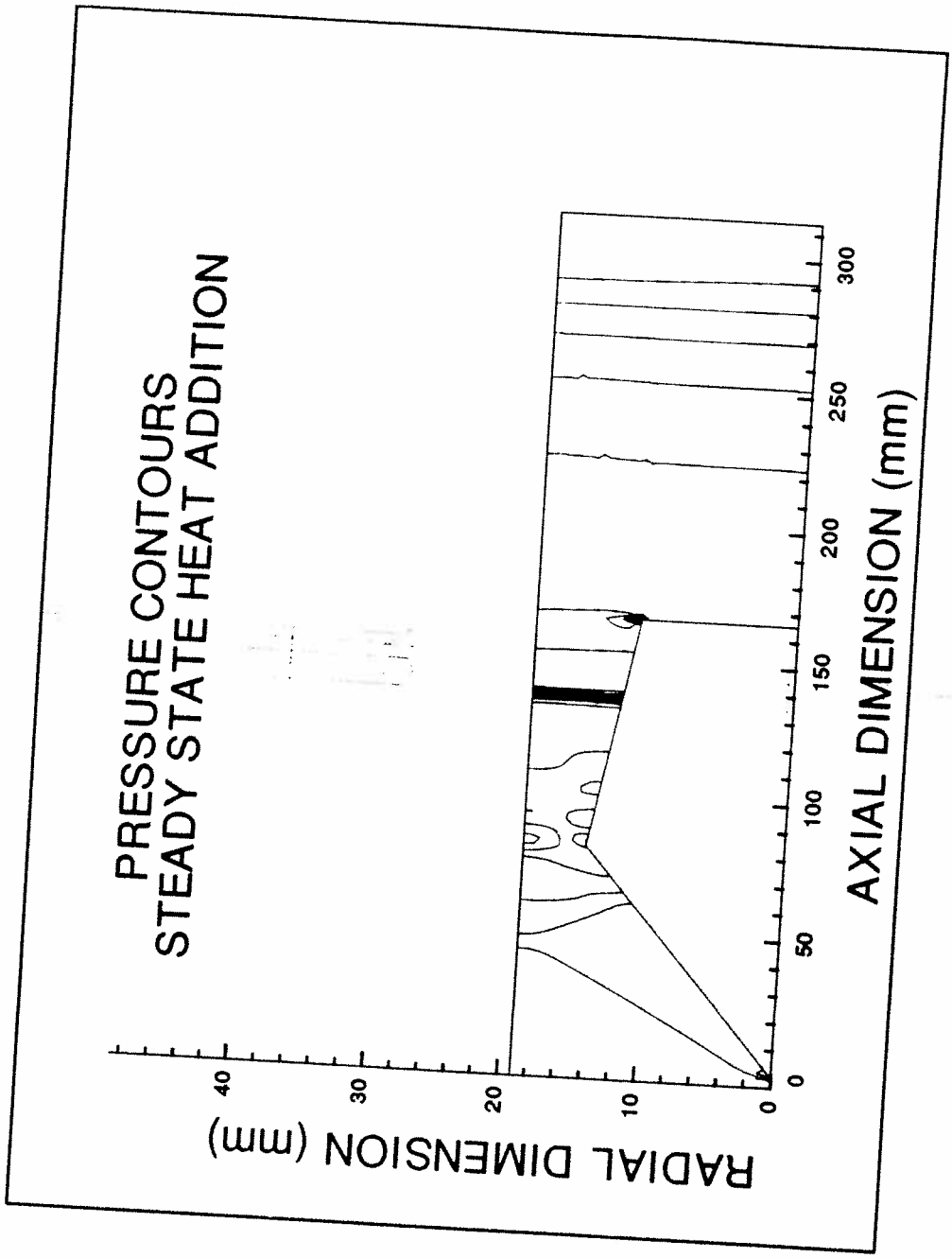

Figure 5.8: Pressure Contours for Vehicle with Steady State Heat Addition

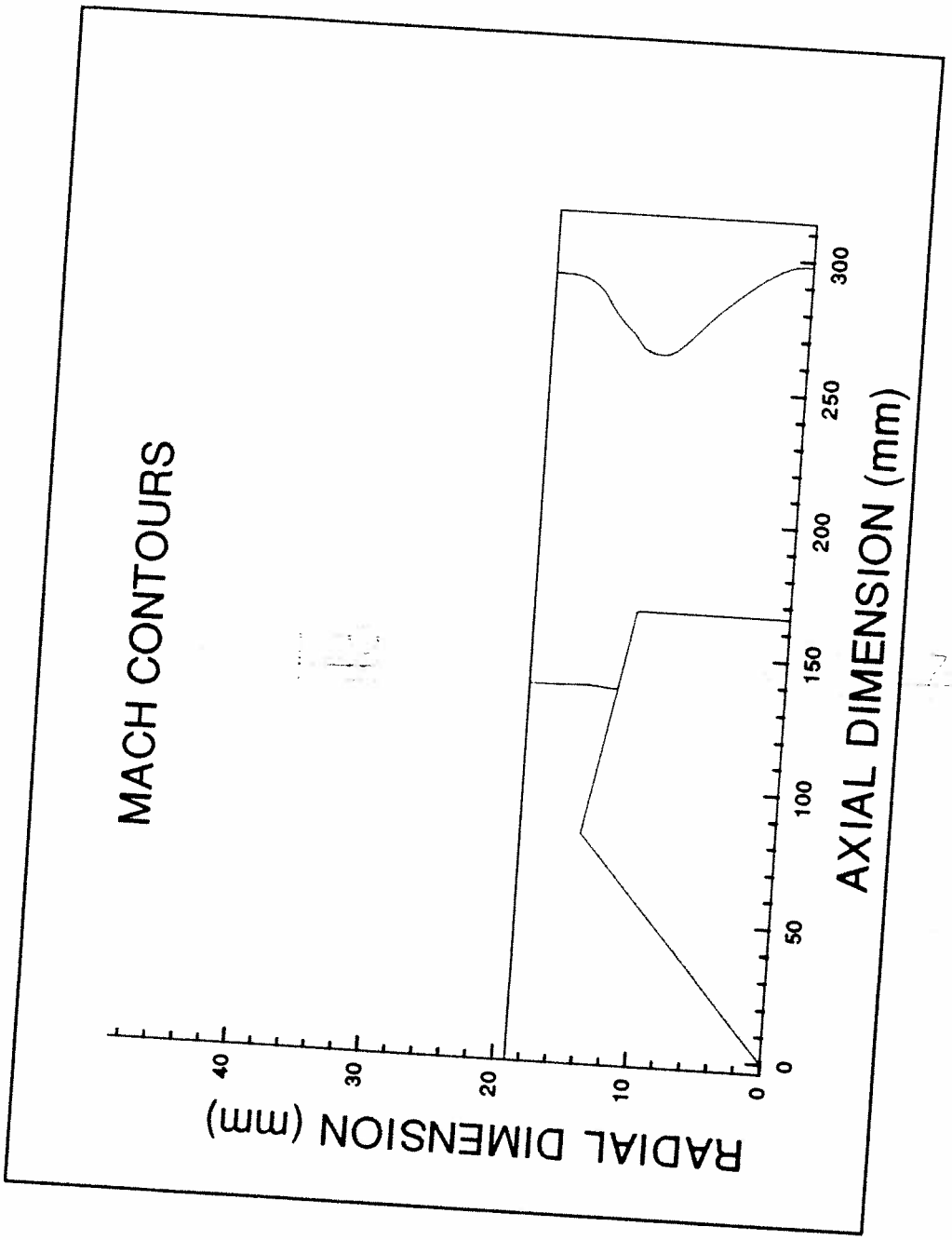

Figure 5.9: Mach Contours for Vehicle with Steady State Heat Addition

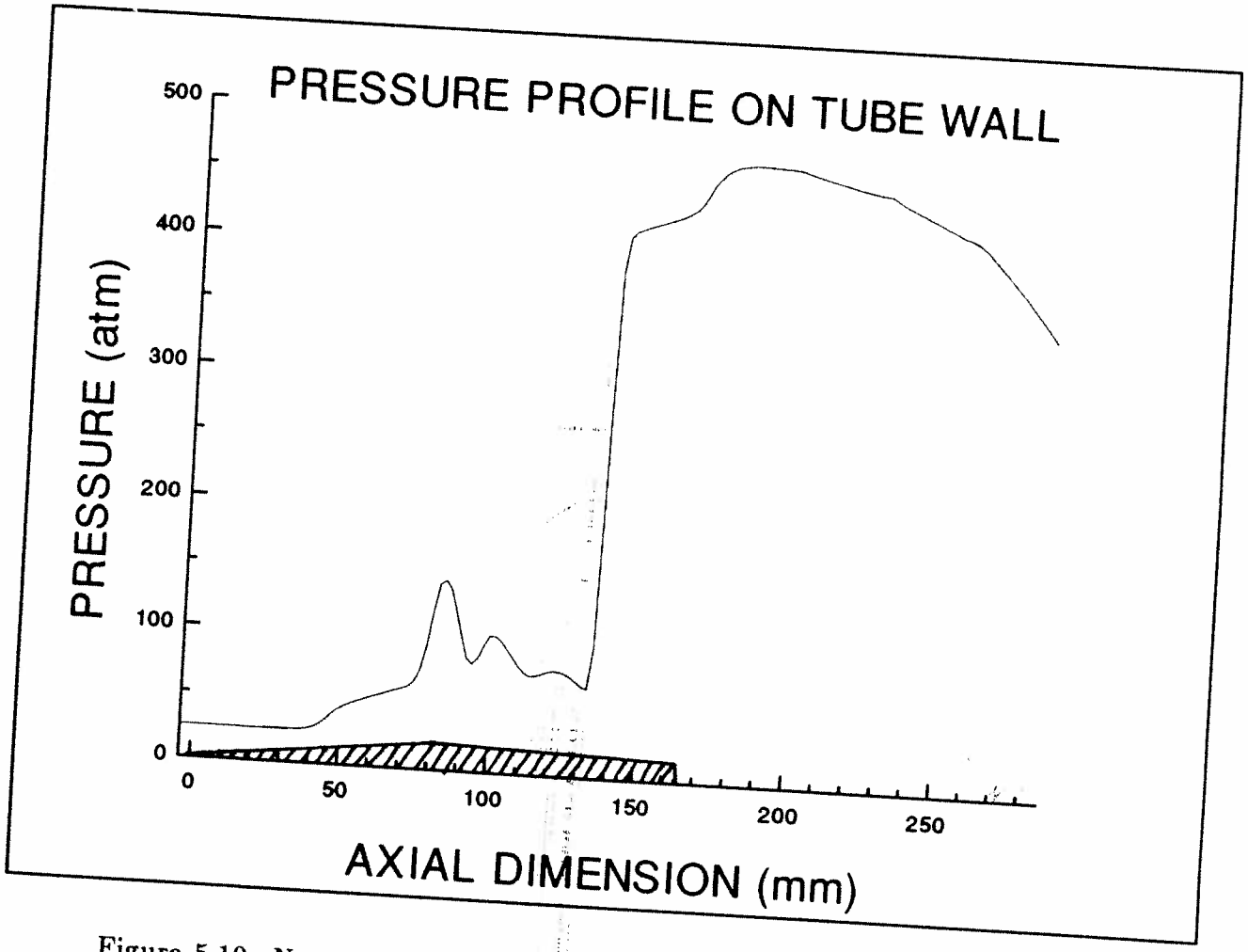

Figure 5.10: Numerical Pressure Profile at Tube Wall for Vehicle with Heat Addition

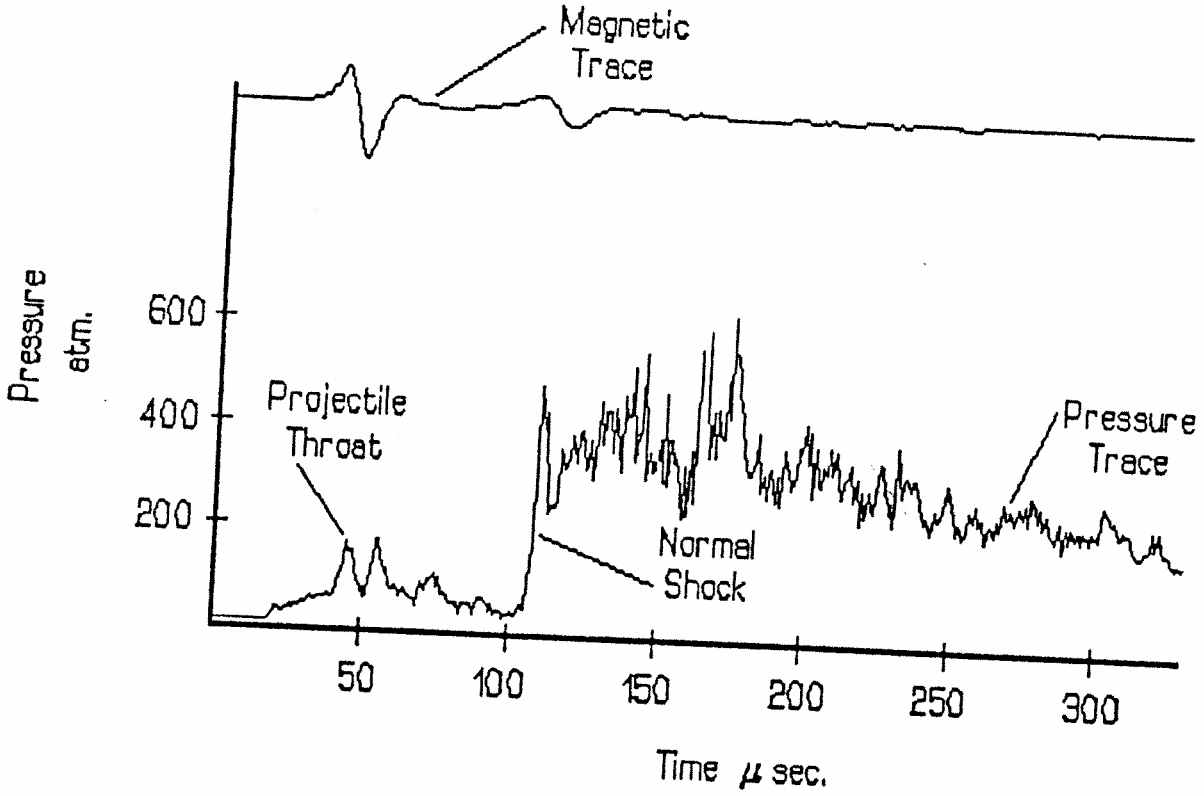

Figure 5.11: Experimental Pressure Profile at Tube Wall

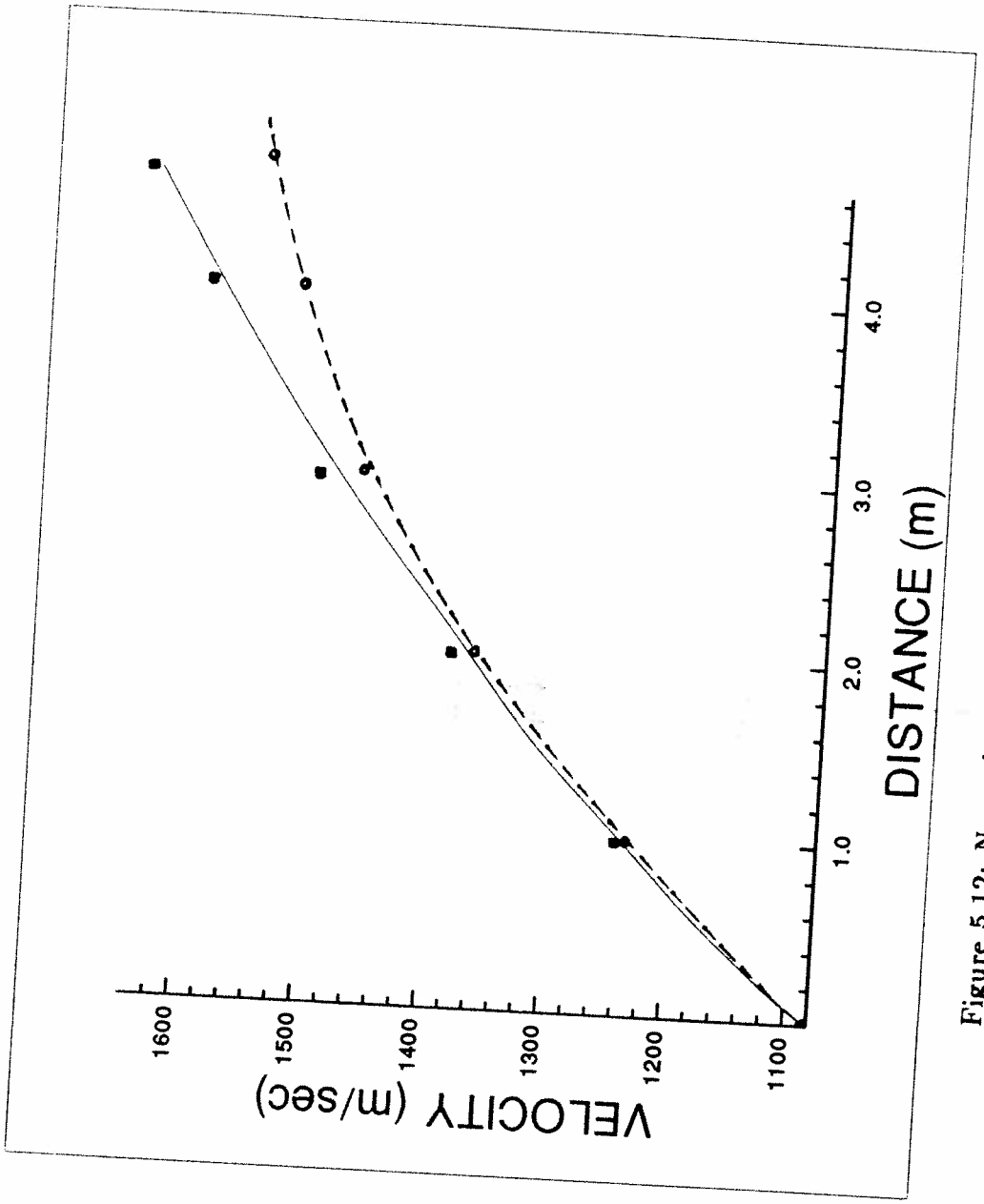

Figure 5.12: Numerical and Experimental Velocity Profile

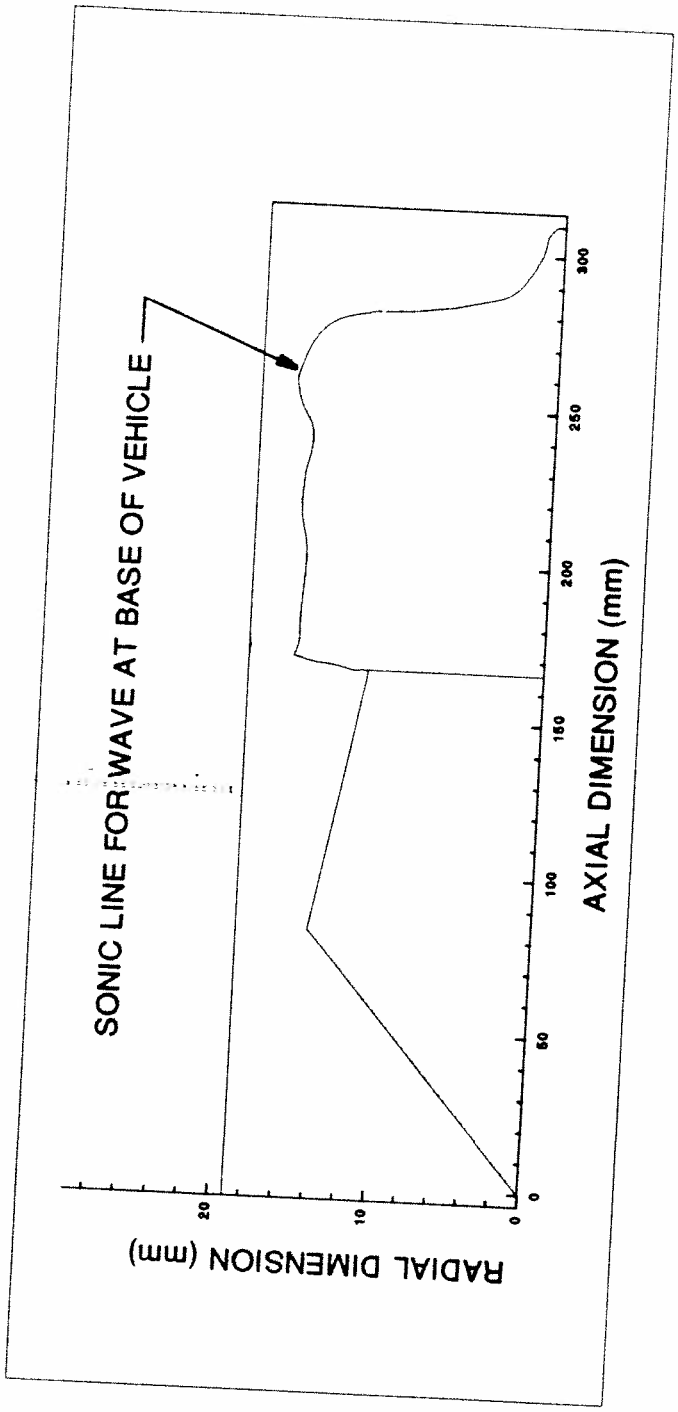

Figure 5.13: Mach Contours for Shock at Edge of Vehicle Body

Chapter 6

Conclusions

6.1 Summary

A nonsteady, inviscid, 2D axisymmetric TVD numerical scheme was presented in order to investigate the flow field about the ram accelerator, and a simple heat addition model was used to model the subsonic combustion thermal choking mode of operation.

Several calculations were performed on the ram accelerator projectile configuration itself. These included supersonic profiles with no heat addition, and cases with heat addition. Although the heat addition model was arbitrarily selected, qualitatively the agreements with experiment were found to be quite good. With selective heat addition the numerical results are in excellent agreement. It was found that the amount of heat release and the location and movement of the heat addition region could affect the results in the unsteady case.

It was determined that the results of the unsteady calculations differ from the quasi-steady model in predicting the thrust on the projectile, and its subsequent acceleration. As the acceleration increased, it was seen that the unsteady thrust was less than that predicted by steady theory. Numerically, the heat added

had to be proportionally increased in order to maintain the acceleration at the higher velocities, or the heat addition region had to change. In addition, the amount of heat that could be added to the flow in the unsteady case exceeded the amount of heat that would cause an unstart in the steady case. This could explain the failure of the quasi-steady model in predicting the operating characteristics at the higher velocity ranges.

The numerical model presented can accurately predict flow fields about the projectile for the case of no heat release, and with the right heat release method the subsonic thermal choking ram accelerator propulsion mode can be well modelled. The model can be usefull for investigating scaling effects, different projectile configurations, different gas mixtures, and even different modes of propulsion.

6.2 Future Work

Because of the ability of the current numerical method to accurately predict flowfields about the projectile, its potential for accurately modeling the ram accelerator subsonic combustion thermal choking mode is excellent. Investigations that need to be performed with the current model include projectile configuration effects, scaling effects, and heat addition model effects. Future work should include investigations of a time dependent heat addition region, where the heat release can be moved forward onto the body to sustain the high thrusts seen experimentally.

Some future issues which need to be addressed include viscosity and turbulence modeling. The addition of the Navier-Stokes terms can address such issues as boundary layer flow and separation of the flow over the discontinuous area change.

Also, the addition of a combustion model can eliminate the need to rely on

arbitrarily selecting the amount of heat to be added to the flow. With the inclusion of species equations and simple chemistry the model could more accurately predict operating characteristics of the thermal choking mode of operation.

Bibliography

[1] Hertzberg, A., Bruckner, A. P., and Bogdanoff, D. W., "Ram Accelerator: A New Chemical Method for Accelerating Projectiles to Ultrahigh Velocities," **AIAA Journal** , Vol. 26, pp. 195-203, 1988.

[2] Bruckner, A. P., Bogdanoff, D. W., Knowlen, C., and Hertzberg, A., "Investigation of Gasdynamic Phenomena Associated with the Ram Accelerator Concept," AIAA Paper 87-1327, 1987.

[3] Knowlen, C., Bruckner, A. P., Bogdanoff, D. W., and Hertzberg, A., "Performance Capabilities of the Ram Accelerator," AIAA Paper 87-2152, 1987.

[4] Bruckner, A. P., Knowlen, C., Scott, K. A., and Hertzberg, A., "High Velocity Modes of the Thermally Choked Ram Accelerator," AIAA Paper 88-2925, 1988.

[5] Bruckner, A. P., Knowlen, C., Hertzberg, A., and Bogdanoff, D. W., "Operational Characteristics of the Thermally Choked Ram Accelerator," to be published in **Journal of Propulsion and Power** .

[6] Kull, A. E., Burnham, E. A., Knowlen, C., Bruckner, A. P., and Hertzberg, A., "Experimental Studies of Superdetonative Ram Accelerator Modes," AIAA Paper 89-2632, 1989.

[7] Hertzberg, A., Bruckner, A. P., and Mattick, A. T., "A Chemical Method for Achieving Acceleration of Macroparticles to Ultrahigh Velocities," Final Report, UWAERP-15, DOE Grant No. DEFG06 85ER13382, Aerospace and Energetics Research Program, University of Washington, Seattle WA, 1987.

[8] Kaloupis, P., and Bruckner, A. P., "The Ram Accelerator: A Chemically Driven Mass Launcher," AIAA Paper 88-2968, 1988.

[9] Bruckner, A. P., and Hertzberg, A., "Ram Accelerator Direct Launch system for Space Cargo," IAF Paper 87-211, 1987.

[10] Yungster, S., and Bruckner, A. P., "A Numerical Study of the Ram Accelerator Concept in the Superdetonative Velocity Range," AIAA Paper 89-2677, 1989.

[11] Burnham, E. A., Kull, A. E., Knowlen, C., Bruckner, A. P., and Hertzberg, A., "Operation of the Ram Accelerator in the Transdetonative Velocity Regime," AIAA Paper 90-1985, 1990.

[12] Yungster, S., "Numerical Simulation of Shock Induced Combustion for Application to the Ram Accelerator Concept," PhD Dissertation, University of Washington, Seattle WA, 1989.

[13] Burnham, E. A., "Experimental and Numerical Analysis of the Thermally Choked Ram Accelerator Starting Process," Master of Science Thesis, University of Washington, Seattle WA, 1989.

[14] Kull, A. E., "Preliminary Investigation of Superdetonative and Transdetonative Ram Accelerator Propulsion," Master of Science Thesis, University of Washington, Seattle WA, 1990.

[15] Lax, P. D., "Hyperbolic Systems of Conservation Laws and the Mathematical Theory of Shock Waves," SIAM Regional Conference Series in Applied Mathematics, No. 11, 1954.

[16] Yee, H. C., Warming, R. F., and Harten, A., "Implicit Total Variation Diminishing Schemes for Steady State Calculations," **Journal of Computational Physics** , Vol. 57, pp. 327-360, 1985.

[17] Roe, P. L., "Generalized formulation of TVD Lax-Wendroff Schemes," Institute for Computer Applications in Science and Engineering, Hampton VA, Report No. 84-20, 1984.

[18] Chakravarty, S. R., Anderson, D. A., and Salas, M. D., "The Split Coefficient Matrix Method for Hyperbolic Systems of Gasdynamic Equations," AIAA Paper 80-0268, 1980.

[19] Anderson, D. A., Tannehill, J. C., and Pletcher, R. A., "**Computational Fluid Mechanics and Heat Transfer** ," Hemisphere Publishing Corporation, New York, 1984.

[20] Yoon, S., and Jameson, A., "Lower-Upper Symmetric Gauss Seidel Method for the Euler and Navier Stokes Equations," **AIAA Journal** , Vol. 26, pp. 1025-1026, 1988.

[21] Jameson, A., and Yoon, S., "Lower-Upper Implicit Schemes with Multiple Grids for the Euler Equations," **AIAA Journal** , Vol. 25, pp. 929-935, 1987.

[22] Yoon, S., Kwak, D., and Chang, L., "LU-SGS Implicit Algorithm for the Three-Dimensional Incompressible Navier-Stokes Equations with Source Term," AIAA Paper 89-1964, 1989.

[23] Shapiro, A. H., "**The Dynamics and Thermodynamics of Compressible Fluid Flow** ," The Ronald Press Company, New York, 1953.

[24] Scott, K. A., "Experimental Investigation of the Ram Accelerator Concept Using an Optical Probe," Master of Science Thesis, University of Washington, Seattle WA, 1988.

[25] Oates, G. C., ed., "**Aerothermodynamics of Aircraft Engine Components** ," American Institute of Aeronautics and Astronautics, Inc., New York, 1985.